TECHNISCHE UNIVERSITÄT WIEN
Vienna University of Technology

Master Thesis

Design, Manufacturing, and Testing of an Open-Source Universal Testing Machine for Hands-On Learning

carried out for the purpose of obtaining the degree of
Diplom-Ingenieur (Dipl.-Ing. or DI),

submitted at TU Wien
Faculty of Mechanical and Industrial Engineering
by

Stella Demmel
Mat.Nr.: 11829503

under the supervision of
Univ.Prof. Dipl.-Ing. Dr.techn. Dieter Pahr
Institute of Lightweight Design and Structural Biomechanics, TU Wien

Vienna, June 2024

Affidavit

I declare in lieu of oath, that I wrote this thesis and performed the associated research myself, using only literature cited in this volume. If text passages from sources are used literally, they are marked as such. I confirm that this work is original and has not been submitted elsewhere for any examination, nor is it currently under consideration for a thesis elsewhere.

I acknowledge that the submitted work will be checked electronically-technically using suitable and state-of-the-art means (plagiarism detection software). On the one hand, this ensures that the submitted work adheres to the high-quality standards of the current rules for ensuring good scientific practice "Code of Conduct" at the Vienna University of Technology. On the other hand, a comparison with other students' theses avoids violations of my copyright.

Vienna, 27$^{\text{th}}$ June, 2024

Stella Demmel

Abstract

In this thesis, a universal testing machine called *MT-02* was designed, built, and tested. The goal was to create a machine that can be used for academic training and demonstration purposes. The specifications of the design include: affordability, portability, ease of extending the soft- and hardware, open-source spirit, and the capability to perform tensile tests as well as compression tests with loads up to 3.5 kN.

Standardized aluminum profiles are used to build the frame of the machine. Low loaded parts were 3D printed. The control is based on an Arduino board. The machine is operated via a touch display and the measurement data is transmitted via a USB interface to a PC.

A tensile test series with plastic samples was performed on the *MT-02* as well as on a commercial universal testing machine. After successfully testing all samples, the results were compared and interpreted regarding the accuracy and precision of the built machine. They indicated a good agreement concerning the strength. The strain of the sample, which is estimated by the displacement of the crosshead, deviates by a factor of two from the results of the commercial universal testing machine with a video extensometer. Thus, the Young's modulus is underestimated by 48 %. Optical strain measurement could resolve this issue.

In summary, this thesis shows that a universal testing machine can be built at well-equipped workshops with a relatively low budget and effort. Measurement outcomes are comparable to commercial test systems.

Kurzfassung

In dieser Arbeit wurde eine universale Zug-Druck-Prüfmaschine mit der Kurzbezeichnung *MT-02* entworfen, gebaut und getestet mit dem Ziel dieses Gerät für Ausbildungs- und Demonstrationszwecke einzusetzen. Die Spezifikationen des neuen Designs waren: preisgünstig, transportabel, leicht erweiterbar, einfache Bedienung, Open-Source-Software und Zug-Druck-Testung mit einer Prüflast bis 3,5 kN.

Der Rahmen wurde aus normierten Aluprofilen gestaltet. Wenig belastete Teile wurden 3D gedruckt und die Ansteuerung erfolgt mit einem Arduino. Die Bedienung wurde mit einem Touch-Display realisiert und die Messdaten werden via einer USB-Schnittstelle übertragen.

Um die Maschine testen zu können, wurde eine Zugtest-Reihe mit Kunststoffproben mit der *MT-02* und einer kommerziellen Universalprüfmaschine durchgeführt. Die Ergebnisse wurden zur Überprüfung der Genauigkeit der gebauten Prüfmaschine verwendet. Es konnten alle Proben mit der Maschine erfolgreich getestet werden. Die Ergebnisse zeigen, dass die Festikeit sehr gut erfasst wird. Die Dehnung, welche über die Querhauptverschiebung abgeschätzt wird, unterscheidet sich im Vergleich zu den Ergebnissen, ermittelt über den Video-Extensometer der kommerziellen Universalprüfmaschine, mit einem Faktor von zwei. Folglich wird der E-Modul um 48 % unterschätzt. Abhilfe kann eine optische Dehnungsmessung schaffen.

Zusammenfassend konnte anhand des Baus der *MT-02* gezeigt werden, dass eine Zug-Druck-Prüfmaschine, welche zu Demonstrationszwecken sowie in der Ausbildung von Ingenieuren eingesetzt wird, relativ kostengünstig und ohne enorme Aufwände in technisch gut ausgestatteten Werkstätten problemlos gefertigt werden kann. Die Messergebnisse sind mit denen kommerzieller Testsysteme vergleichbar.

Acknowledgments

First of all, I would like to thank my supervisor Prof. Dieter Pahr for the opportunity and trust to realize this project. Thank you for your patience as well as the ideas and suggestions concerning the design of the machine.

A big thank you to Maria Grill for not letting us get insane with the restrictions while ordering the needed parts and coming up with little strategies to outsmart failed algorithms after trying to find the right part for hours. An immense appreciation for the whole team of the institute for their kindness and support. Whenever a problem came up, everyone gladly offered to help.

Thank you, Fabi, for converting the workshop into a photo studio for a day and producing the most beautiful pictures of the machine. Thank you for always being there for me and for not letting me despair with certain image manipulation programs not working the way I would like them to.

I would like to thank my whole family and friends for always supporting me and listening to my problems. A huge *Mitarbeitsplus* for Robert, for sparing no effort to help me and for making it possible to introduce myself to 3D printing in the first place.

And of course, the deepest gratitude to Robert Exler, who always supported me and my ideas, for trusting me and guiding me through his workshop. Thank you for machining every part of the machine, that I could not or was not allowed to do myself, and for taking the time to explain every step on the way.

Contents

Nomenclature

Acronyms

CAD computer-aided design

CPU central processing unit

DIP dual inline package

EEPROM electrically erasable programmable read-only memory

FDM fused deposition modeling

I^2C inter-integrated circuit

LCD liquid-crystal display

NEMA National Electrical Manufacturers Association

PCB printed circuit board

PETG polyethylene terephthalate glycol-modified

RAM random access memory

RPM revolutions per minute

TFT thin-film transistor

TPU thermoplastic polyurethane

UTM universal testing machine

List of Figures

List of Tables

1. Introduction

Universal tensile and compression testing machines (Figure 1) are used for the mechanical testing of material samples or structural components. Such machines are expensive to purchase and maintain, training is time-consuming, and sufficient experience is required to use such test systems. Well-equipped laboratories operate such machines, but such testing systems are only available to a limited extent in general.

Figure 1.: *Typical universal testing machine: ZwickRoell AllroundLine [1]*

These circumstances lead to restrictions in various technical areas where an inexpensive, widely available material testing machine can provide a remedy. In materials science education, for example, the focus is often on theory, and practical experience in the use of such equipment is often neglected. Another example is 3D printing where a material is constantly being produced which reacts very sensitively to changes in process parameters and ongoing material testing is useful. Furthermore, in the field of biomedical engineering, very specific tasks can be required in addition while performing a material test. For instance, synchronous temperature, pH value, or fluid sensors need to be used as well. A testing machine with an open architecture into which such sensors can be integrated is therefore very useful.

Most universal testing machines available on the market nowadays weigh between 55 kg [2] and 2100 kg [1] (Figure 1). This means that once they are set up they usually are not moved anymore. If they are moved, a recalibration of the system is necessary. This is accompanied with additional costs and consumes time. Furthermore, an official introduction is required to operate the machine due to safety issues, and if such equipment is damaged, the replacement and repair is expensive. Therefore, a lightweight material testing machine with relatively cheap parts would have the ability to fill this gap.

Some do-it-yourself testing machines are already available online. Those are open-source and designed for material testing at home. Mostly wood or 3D printed plastic is chosen as the main components for the design (Figure 2a and Figure 2b). This design only allows rather low maximum permissible loads. Furthermore, the use of cheap electronic devices and rather weak motors limits the field of use even more. In addition, the handling of those do-it-yourself testing machines is rather inconvenient. Only buttons or a connected computer are used for their operation [3, 4].

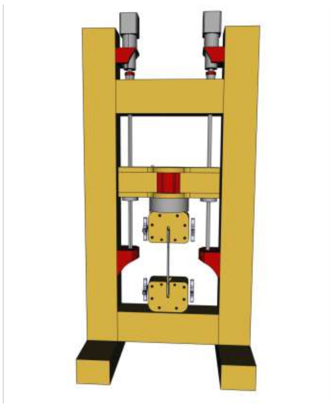

(a) *CAD model of the Open-Pull universal testing machine by Stefan Hermann [3] with wooden parts (dark yellow) and 3D printed parts (red)*

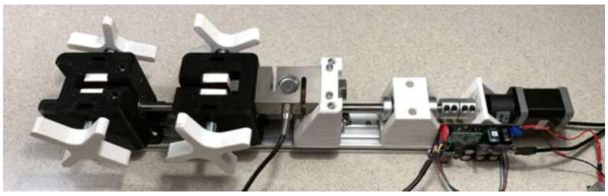

(b) *Universal tensile testing machine by Xieshi Zhang [4]*

Figure 2.: *Open-source material testing machines currently available*

Based on these limitatoins, the mechanical testing machine called *MT-01* was developed by Dr Pahr Ingenieurs e.U. (Pfaffstätten, Austria). Its design is based on aluminum profiles, a special Nema 23 stepper motor, an Arduino controller, linear rails, and 3D printed parts. The maximum permissible load of this system is 1.5 kN (Figure 3). The handling is quite convenient by using a momentary rocker switch and an encoder. A small LCD screen shows the parameters and the main results of the test. A computer needs to be connected via USB to the testing machine to extract more specific information. This means that still a testing machine with an even higher user-friendliness and range of applications is of great interest.

This master thesis is a further development of the MT-01 material testing machine. It covers the design and construction of a material testing machine, called *MT-02*. Its fundamental purpose is for demonstration and teaching applications, where the

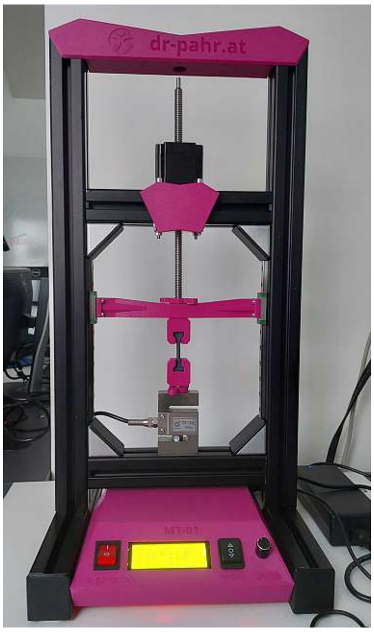

Figure 3.: *MT-01 developed by Dr Pahr Ingenieurs e.U. (Pfaffstätten, Austria), the pink parts are 3D printed*

highest accuracy is not crucial. As most material testing machines on the market are quite expensive and can be very complex to operate, the *MT-02* can be used as a cheap alternative to teaching students the basics of material testing. Moreover, this machine can be used for any application, where the highest accuracy is not of the greatest significance, but easy-to-use and transportable design is important. As it is considered an open-source machine, the software can be modified and extended to fulfill other needs.

The main objective was to use the knowledge gained from Biomedical Engineering courses regarding material testing as well as engineering mechanics, informatics, additive manufacturing, and electronics to develop the *MT-02* testing machine. This interdisciplinary field of study is highly versatile, providing an ideal foundation for constructing and implementing all the necessary software for the material testing machine. The operation of the machine is designed closely to the needs of the user. This was achieved by always having the actual application of the machine in mind and by exactly knowing what is of importance, just like how the specimens of interest are prepared and how the results are interpreted.

As a proof-of-concept, a testing series on 3D printed samples was done in this thesis and compared to a commercial universal testing machine (UTM). Force and displacement outcomes were compared to get a feeling of the quality and usability of the *MT-02* material test system.

2. Background

2.1. Mechanical Testing

Universal testing machines facilitate the testing of materials and structures under mechanical loads. These machines check the load capacity of those materials and structures by recording the load and the change in shape. It is differentiated between tensile, compression, and bending tests [5]. In this section tensile testing is described in greater detail, as this type of test is performed in this thesis.

Two typical types of machines are used to perform static tensile tests: electro-mechanical and servo-hydraulic testing machines. Electro-mechanical testing machines are typically smaller. They are driven by electric motors and gears. In contrast, servo-hydraulic testing machines use pressure cylinders and are able to apply forces up to 2000 kN [5].

Universal electro-mechanical testing machines (Figure 4) consist of a fixed part and a movable part, also called a crosshead. The position and speed of the crosshead are precisely controlled. The crosshead is typically guided by linear rails to eliminate any deviation from the desired position. A load cell is used to measure the load, which is exerted on the sample during the test. This load cell is attached to the fixed part of the machine.

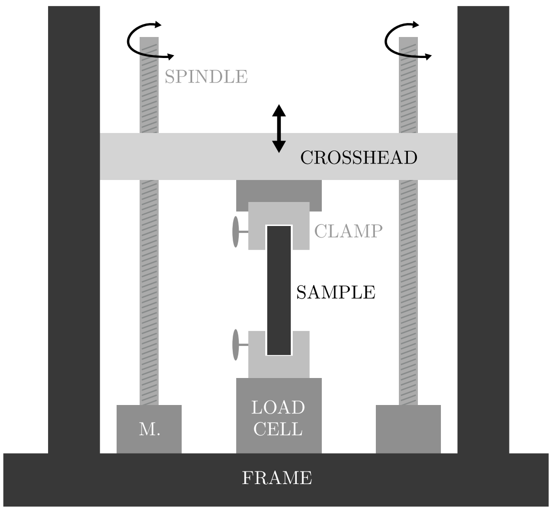

Figure 4.: *Sketch of a universal testing machine including the frame, the moving crosshead, the spindles rotating due to the motor (M.), the sample fixed to the clamps by screws, and the load cell*

A sample is considered as the part that is being tested. Standardized geometries of the samples enhance the comparability of different tests. Different standards are used for different types of applications. The shape of the samples ranges from rectangular dog bone shape to short cylinders [6]. For example, the dimensions for metal samples are described in *DIN 50125: Testing of metallic materials - Tensile test pieces* [7] and *DIN 50106: Testing of metallic materials - Compression test at room temperature* [8], for tensile and compression testing respectively. *ISO 527-1: Plastics — Determination of tensile properties — Part 1: General principles* [9] characterizes the shape of tensile test samples made of plastic.

Test scenarios include quasi-static, dynamic, and cyclic testing. Quasi-static testing is performed at low speeds, i. e. low velocities of the crosshead, and dynamic testing at strain rates over $0.1\,\mathrm{s}^{-1}$ [10]. Another type of testing addresses the material behavior under stationary load. Those stationary tests consist of the creep test and the stress relaxation test. The test force is kept constant over a certain amount of time, while the deformation is measured, to characterize the creep of the material. The relaxation of a sample is determined by keeping the deformation constant and measuring the decrease in force [6].

Tests are either performed displacement or strain controlled or force controlled. This means that for a displacement or strain controlled test, the displacement or strain is changed precisely as a function of time. Whereas the force or stress is adjusted based on time during a force or stress controlled test. The other quantity is then measured and interpreted, respectively [6].

The values, which are measured during a test, are the force and the elongation of the sample. A load cell is used to quantify the force, which is acting on the sample. In modern setups, the measured data is directly plotted as a graph on a computer by employing specific software. The elongation is determined by either using the distance the crosshead travels or with the help of an extensometer. This extensometer is an electrical device, which is clamped directly onto the sample during the test. It measures the distance between its two clamps based on induction [5].

Testing standards are established to compare results more easily. Various characteristics like the shape of the sample, the testing speed, and characteristic values used for the analysis are described in those particular standards [6]. Nevertheless, there are still numerous factors that challenge the comparison like the composition of the material and the environmental conditions while the sample was prepared and tested [11].

Specific values are established in material testing to analyze the material characteristics and compare the results. The following paragraphs describe the most important values in the context of tensile testing.

The nominal tensile stress or engineering stress, σ, is calculated based on the force, F, and the initial cross-sectional area, A_0, of the sample in the region of the gauge length [12]:

$$\sigma = \frac{F}{A_0}. \tag{1}$$

The gauge length is the middle part of a sample in which the cross-sectional area is constant [12].

True stress is the force in relation to the actual cross-sectional area, rather than the initial cross-sectional area. Therefore, the value of true strain is significantly higher than the value of the nominal tensile stress, as the current cross-sectional area starts to decrease during the tensile test. This is especially true, when necking occurs [5].

The strain or engineering strain, ε, is calculated by dividing the change in length, ΔL, by the original length, L_0, of the region of the gauge. Therefore, the strain is dimensionless and represents the ratio of elongation [12].

True strain, on the other hand, is the actual change rate in the momentary gauge length. This true strain, ε_T, is calculated based on the momentary length of the specimen, L, and the initial length, L_0, or on the engineering strain, ε_E, [13]:

$$\varepsilon_T = ln\left(\frac{L}{L_0}\right) = ln\left(1 + \varepsilon_E\right). \tag{2}$$

True stress and true strain are essentially identical to the engineering stress and strain measures at small deformations. The values only start to differ drastically, when the deformations increase [13].

The tensile strength, R_m, is calculated similarly to the tensile stress but with the use of the maximum force, F_max, [12]:

$$R_\mathrm{m} = \frac{F_\mathrm{max}}{A_0}. \tag{3}$$

The modulus of elasticity, E, is determined as the slope of the linear part of the stress-strain curve [12]. Figure 5 shows a graph of a force-elongation or a stress-strain curve as obtained by a tensile test visualizing the specific values.

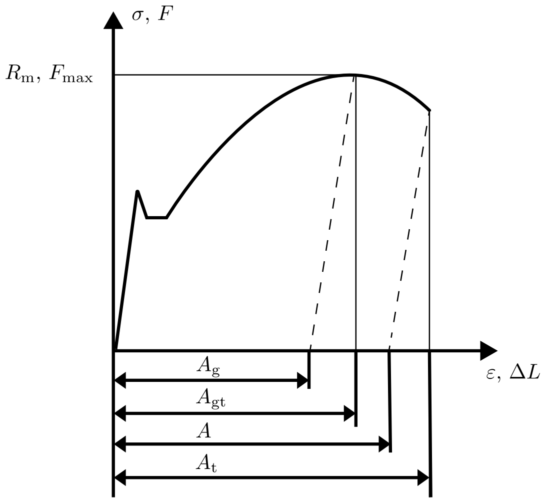

Figure 5.: *Schematic graph as a result of a tensile test, adapted from Schöggl [5]*

2.2. Precursor Universal Testing Machine MT-01

A first version of a light weight and affordable universal electro-mechanical testing machine was designed by Prof. Pahr (Dr. Pahr Ingenieurs e.U., Pfaffstätten, Austria). It is called *MT-01* and was used as the main inspiration for the *MT-02*. Figure 3 shows the *MT-01* equipped with clamps for tensile testing. The computer-aided design (CAD) model is depicted in Figure 6.

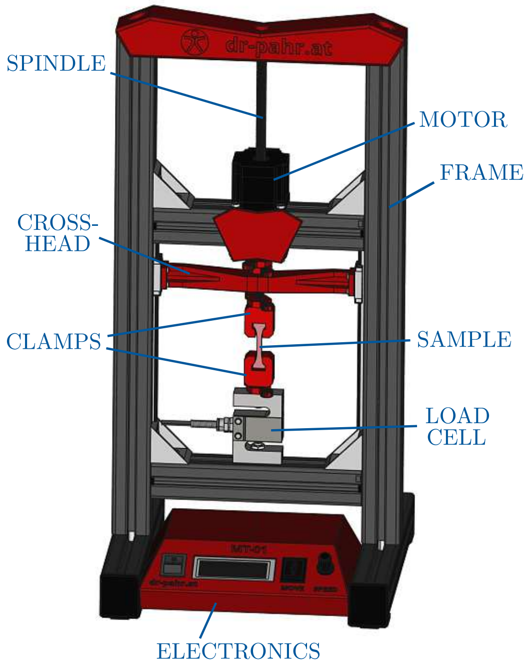

Figure 6.: *CAD model of the MT-01 by S. Rauner, ILSB*

The design is very convenient regarding the construction and potential further modifications. The machine is portable and able to perform tensile or compression tests with loads up to 1.5 kN. The crosshead can be moved with a speed in the range from 0 05 to 10 mm s^{-1}.

The frame is constructed with aluminum profiles with a cross-section of 40 mm x 40 mm. Moreover, some parts like the top or the crosshead are 3D printed from polyethylene terephthalate glycol-modified (PETG) (the red parts in Figure 6). The electrical components, which are located in the electronics box under the lower beam, include the *Arduino* microcontroller board that is used as the controlling unit. The stepper driver is needed to supply the stepper motor with sufficient power. The stepper motor is attached to the middle aluminum beam and uses the spindle to move the crosshead, which is attached to the bottom of the spindle. The S-shaped load cell is fixed to the lower beam. It is capable to record load data up to 200 kg.

Figure 7 shows the electric circuit of the *MT-01*. It consists of the following components:

- Microcontroller board
- Display
- Step down module
- Load cell
- Analog-to-digital converter
- 24 V power supply
- Stepper motor
- Stepper motor driver
- Switch
- Rotary encoder

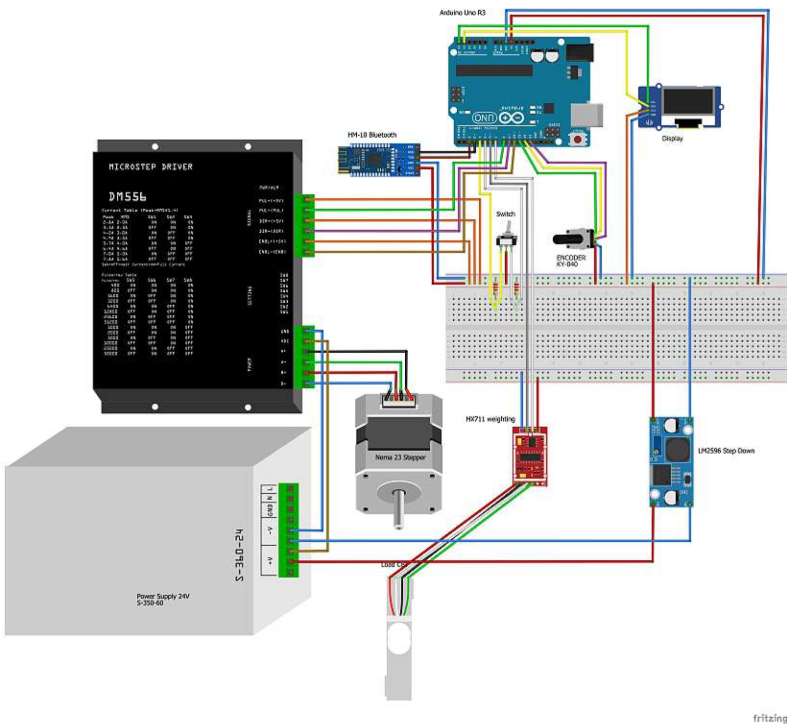

Figure 7.: *Circuit diagram of the MT-01 by Prof. Pahr (Dr. Pahr Ingenieurs e.U., Pfaffstätten, Austria)*

Operating the *MT-01* is quite easy. One rocker switch is used to power the machine on or off and another one controls the movement of the crosshead. The speed of the crosshead is set With the help of a rotary encoder. The speed needs to be chosen under a threshold of $0.4\,\mathrm{mm\,s^{-1}}$ to record data. The switch needs to be pressed upwards or downwards to start the test, according to whether a tensile or compression test is desired. As long as the switch is held in this position, the live information about the duration, the load, and the travel data is printed to the liquid-crystal display (LCD) screen. The serial port is used to export this measurement data. This is achieved by connecting a computer to the Arduino via USB. It is recommended to use the free software *PuTTY*, which logs all serial data in a text file.

As soon as the switch is released again, the measurement ends and the LCD screen displays the maximum load as well as the maximum travel data. When the speed of the crosshead is over the threshold, the *travel mode* is activated. This means that the crosshead is only moving, when the up/down switch is pressed. However, no measurement data is recorded.

Nevertheless, the field of use of the machine is limited due to the National Electrical Manufacturers Association (NEMA) 23 stepper motor with the integrated trapezoidal spindle, as the stepper motor only allows load applications up to 1.5 kN. Furthermore, this type of stepper motor and spindle is rather expensive in comparison to a stepper motor with a shaft and a separately purchased spindle. Moreover, performing cyclic loading is not advisable. This is due to the fact that the clearance of the trapezoidal spindle and nut system is larger, than a ball screw system for example.

To sum up, the *MT-01* represents a simple and portable universal testing machine. Still, some improvements especially concerning the maximum permissible load and the user-friendliness can be made. A more powerful motor or two motors acting synchronously have the potential to increase the maximum load. Moreover, a cyclic testing function can be added by choosing a spindle with a reduced clearance. Improving the user experience can be achieved by replacing the rocker switch as well as the rotary encoder with a touch display. Ideally, this LCD provides an increased size, resolution, and color display.

2.3. Main Components

Figure 7 shows the main electrical devices needed for a mechanical testing machine. These include a microcontroller, a motor, and a load measuring device. The Arduino microcontroller is used as the main controlling part of the system. It manages every electrical part of the machine and records the data. The stepper motor actuates the moving part of the testing machine. The load cell measures the load data, which is then transferred to the microcontroller. Those parts are described in more detail in the following subsections.

2.3.1. Stepper Motor

A stepper motor characteristically subdivides the rotation of its shaft into discrete steps. A step is triggered by an electrical impulse, allowing a precisely controlled movement via a signal generator or a microcontroller for example. Therefore, they typically are put to use, where a well defined movement and position of the moving part is needed.

The basic structure of a stepper motor consists of a stator and a rotor, which are both teethed to increase the resolution and thus decrease the stepping angle [14]. There are three main types of stepper motors. Figure 8 shows sketches of the three different types.

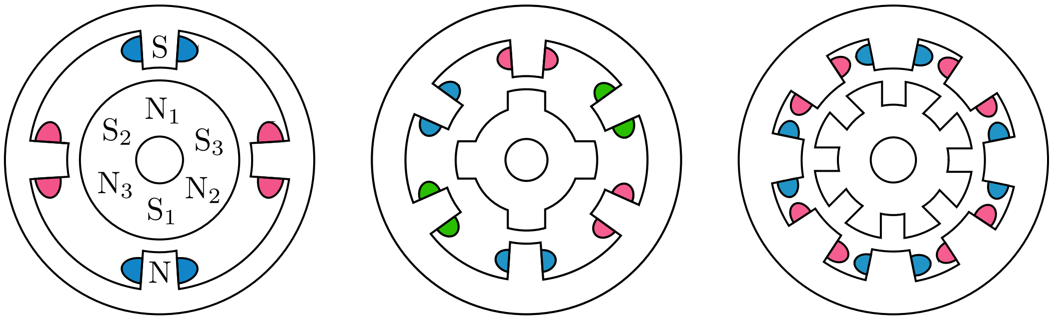

(a) *Permanent magnet stepper motor adapted from Hernández-Guzmán et al. [15]*

(b) *Variable-reluctance stepper motor adapted from Rahman et al. [14]*

(c) *Hybrid stepper motor adapted from Rahman et al. [14]*

Figure 8.: *Sketch of the cross-section of different stepper motor types*

One type is the permanent magnet stepper motor. It consists of a coiled stator (outer part in Figure 8a) and a permanent magnet as a rotor (inner part in Figure 8a). Variable-reluctance stepper motors are characterized by their unexcited rotor, which is attracted by the magnetic field induced by the stator. Its step angle, θ, (in °) describes the angle that the shaft of the stepper motor rotates with one step. The step angle is calculated based on the number of phases (colored parts in Figure 8b), N, and the number of poles, P, in the stator [14]:

$$\theta = \frac{360}{N \cdot P}. \tag{4}$$

A hybrid stepper motor combines the features of both, a permanent magnet stepper motor and a variable-reluctance stepper motor. This results in increased resolution and torque. This is achieved by using a permanent magnet rotor, magnetized in the direction of the rotational axis. At both ends along the rotational axis, a toothed disk made out of soft iron is attached, respectively. This structure allows a concentrated magnetic circuit to form within the teeth [16].

Two different types of drive circuits are commonly used to control the operation of a stepper motor. The simpler type, the unipolar drive (Figure 9a), is preferred for variable-reluctance stepper motors. This is due to the fact that for variable-reluctance stepper motors only the amplitude of the current but not its direction of flow influences the generated torque. On the other hand, a bipolar drive (Figure 9b) is used to have the current flowing through the coils of the stator alternating in both directions. This circuit poses a greater challenge during manufacture. Nevertheless, this type of drive is highly favored for permanent magnet and hybrid stepper motors, as the polarity is of great importance [14]. Basic unipolar drives only consist of a diode wired in parallel to the winding and a transistor connected in series. A bipolar drive is implemented via a bridge drive consisting of four diodes and four transistors, which are each connected in parallel and linked in series to the winding [14].

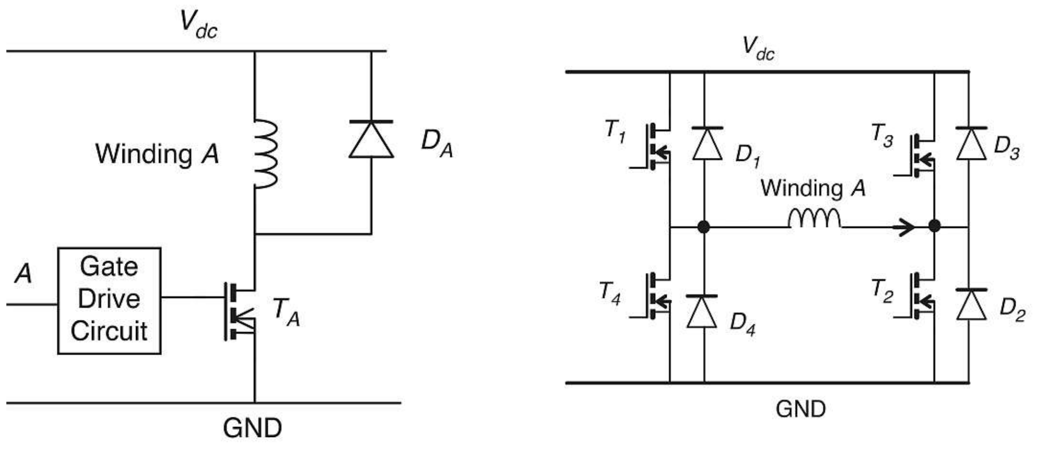

(a) *Unipolar drive circuit* (b) *Bipolar drive circuit*

Figure 9.: *Types of electric circuits for stepper motors from Rahman et al. [14]*

Some important factors by which a stepper motor is characterized, should be found in its datasheet and considered before using the stepper motor in any setup. Those factors constitute of the step angle, the holding torque, and the maximum permissible current amplitude per phase. The step angle, θ, can also be converted in steps per revolution:

$$SPR = \frac{360}{\theta}. \tag{5}$$

The steps per revolution represent an essential value for computing the movement of the shaft of the stepper motor. The position of the shaft can be calculated based on the initial position, the steps per revolution and the number of performed steps. The holding torque embodies an interesting value for the dimension of a system with a linear actuator. The position of the moving system can only be described and controlled precisely, if the stepper motor does not skip a step. Especially in the case that the load on the system exceeds its permissible maximum, the signal provoking a step is potentially ignored by the stepper motor. This results in no movement of the stepper motor shaft all.

The National Electrical Manufacturers Association (NEMA) provides a standard for stepper motors regarding their size [17]. Following the standard, the stepper motors are classified in groups depending on their width (or length, as their cross section is quadratic). The name of a group is defined by the width of the frame in inches divided by a factor of 10. Some commonly used stepper motor sizes are the Nema 11, the Nema 17, and the Nema 23, specifying a frame with a width of approximately 1.1 in, 1.7 in, and 2.3 in, respectively.

2.3.2. Gearbox

Gearboxes are used to modulate on the one hand the linear or rotational speeds and on the other hand the torques or forces of motors. Different types of gearboxes include the spur gear, the screw or spindle drive, and the planetary gear [18].

In spur gears, the drive shafts are aligned in parallel. Gear wheels are attached to the shafts such that the gear teeth mesh with each other. The number of teeth is used to determine the magnitude of the torque being transmitted from the first drive shaft to the second, M_2:

$$M_2 = \frac{N_2}{N_1} \cdot M_1 \tag{6}$$

with the number of teeth on the first gear wheel, N_1, and on the second one, N_2, as well as the torque on the first drive shaft, M_1 [18].

A screw or spindle drive converts a rotational movement into a linear movement. The lead of the screw or spindle, l, controls the magnitude of the converted force and speed. The linear speed, v, is calculated as:

$$v = l \cdot \omega \tag{7}$$

based on the angular velocity, ω, [18].

The planetary gear allows speed conversions without disrupting the flux of force. These gearboxes consist of multiple coaxial shafts with one sun gear in the center. The planet gears travel around the sun gear within a ring gear, which is the outermost part of the gear set [19].

The gear ratio describes the ratio of teeth between the output and the input gear wheel. A gear ratio of 2:1, for example, indicates that the number of teeth on the output gear wheel is twice as high as on the input gear wheel. A higher gear ratio results in higher output torques. However, the speed is linked inversely proportional to the gear ratio. This means that gearboxes with higher gear ratios also reduce the output speed [16].

2.3.3. Stepper Driver

A stepper driver is used to regulate a stepper motor. Figure 10 shows two different stepper drivers. In Figure 10a the *A4988* on a board is depicted together with a sketched wiring diagram. The stepper driver *DM542T* in Figure 10a represents a much more sophisticated type of driver [20]. Compared to the *A4988*, the *DM542T* is much bigger and intended for the use with more powerful stepper motors.

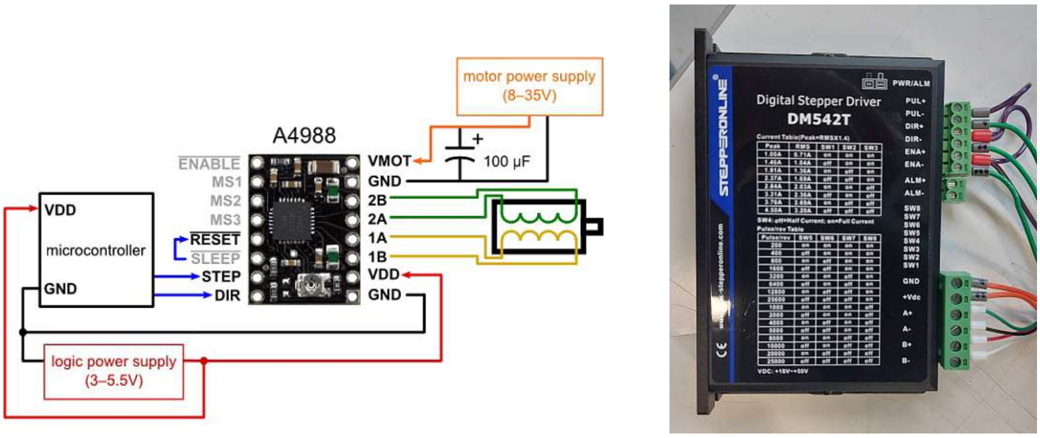

(a) *Wiring diagram of the A4988 stepper driver [21]*

(b) *DM542T stepper driver*

Figure 10.: *A selection of stepper drivers*

Just like most modules, stepper drivers are equipped with ground pins and power pins (Figure 10a). The power pins include a pin for the voltage of the driver itself (around 5 V) and one for the stepper motor (around 24 V). Typically, stepper drivers have input pins for the control of the steps, the direction of rotation, and for disabling the motor. A microcontroller is connected to those input pins and is able to operate the motor via signals to the pins. Two output pins for each phase of the connected bipolar stepper motor are present [21]. The current for the motor is provided via those pins. The driver regulates this current depending on the control signal from the microcontroller containing the settings for the direction and speed of the rotation of the motor shaft. The stepper motor then performs steps based on this current signal.

Microstepping is a technique to refine the motor control. It modifies the current waveform from a basic square wave to an approximation of a sine wave (Figure 11). This increases the number of steps per revolution by subdividing one step into smaller steps. Thus, the resolution of the rotor motion increased [22].

In microstepping, the current reaches 100 % of the configured current only at the peak of the approximated sine wave during one microstep. During the rest of the signal, the current is lower. This reduction in current diminishes the holding torque, as presented in Table 1 [24]. Consequently, no microstepping, or a microstepping resolution of 1, maintains the original holding torque without any decrease.

Table 1.: *Holding torque depending on the microstepping resolution [24]*

Microstep resolution	1	2	4	8	16
Holding torque per microstep in %	100	70.7	38.3	19.5	9.8

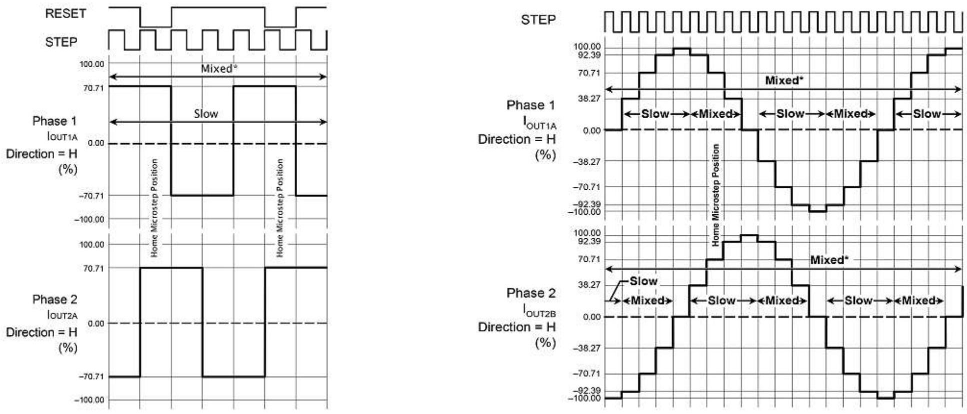

(a) *Current signal using full step and the corresponding step signal [23]*

(b) *Current signal using a fourth microstep and the corresponding step signal [23]*

Figure 11.: *Sketch of the current flowing through both windings of a stepper motor comparing full step and microstepping*

2.3.4. Arduino

An *Arduino* is an open-source microcontroller board. A microcontroller consists of a central processing unit (CPU), the memory, and the peripherals. The CPU acts as the *Brain* of the microcontroller. This means that it performs all needed arithmetic operations. The memory can further be differentiated between the random access memory (RAM) and the flash memory. The RAM only stores data temporarily and is very fast accessible. The flash memory, on the other hand, stores data even after restarting the microcontroller and is usually bigger than the RAM. The peripherals include all parts of the microcontroller, which are neither CPU nor memory. Pins are for example an important part of the peripherals. They are used as an interface between the microcontroller and other devices [25].

A very versatile *Arduino* microcontroller board model is the *Arduino UNO R3* (Figure 12). It is a board with the ATMEGA320P microcontroller as its main component. All parts needed to run and use the microcontroller in basic setups are present on the board as well. The dimensions of the board are standardized. This means that various projects and shields are compatible with the *Arduino UNO R3*. Shields are different boards that allow easy access to the pins on the *Arduino* board [26].

Arduino offers a variety of microcontroller boards and shields besides the *Arduino UNO R3*. The *Mega family*, including the *Arduino Mega 2560 Rev3* board, is designed for projects with the need for high computational power as well as additional in/out pins. In contrast, the *Nano family* offers a multitude of additional sensors and communication modules condensed on a small surface [28]. This is of convenience for applications with restricted space.

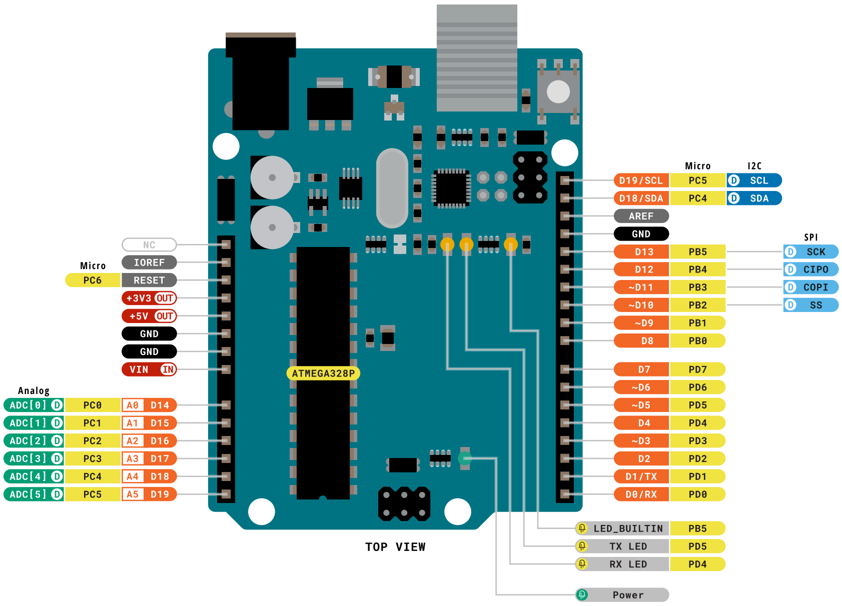

Figure 12.: *Schematic of the Arduino UNO R3 Board with the ATMEGA320P microchip (in the middle of the board), in/out pins (orange), power pins (red), and ground pins (black) [27]*

2.3.5. Display

A display allows the user to perceive an image signal as a two dimensional image. LCD is a very common technology to achieve this conversion. A LCD consists of a light source, which is also called the backlight, and a liquid crystal layer (Figure 13). This layer modulates the light from the light source in response to an electric field. When the LCD is powered on, the light source always emits the same light. This means that even if an LCD is only showing a black screen, the backlight still requires the same energy as if a fully white screen was shown. The liquid crystal layer makes the difference in the appearance by blocking all this light. A color filter is added to the LCD in the case of a color display [29].

Polarizers play an important role during the pathway of the light in the LCD, as depicted in Figure 13. They filter out light, which is polarized in a certain way. Typically, the polarizer after the liquid crystal layer only lets light pass though, which is oriented perpendicularly to the light coming through the first polarizer. So, if there were no liquid crystal layer between both polarizers, no light would reach the display cover. However, the liquid crystals have the ability to change the orientation of the light up to 90°, thereby controlling the amount of light reaching the cover. Here, the thin-film-transistor (TFT) comes into play. Each transistor located at each pixel controls the current to a small capacitor based on the image input signal. This capacitor changes the electric field and thus the magnitude by which the light orientation is modified by the liquid crystals [29].

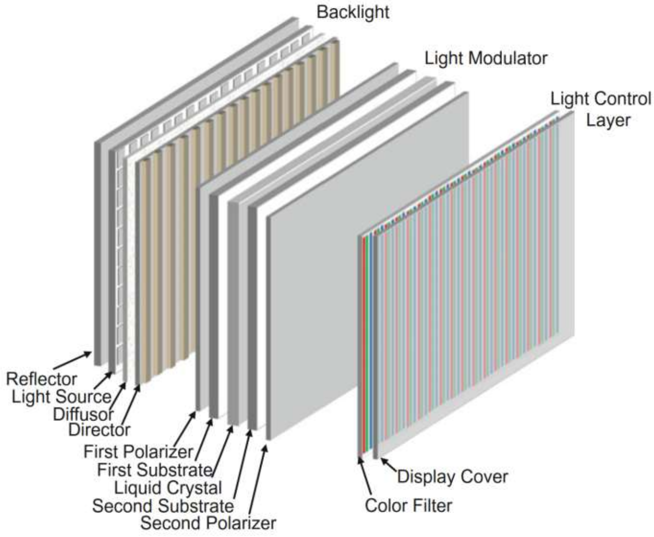

Figure 13.: *Structure of an LCD [29]*

2.3.6. PCB

In the process of prototyping, the electric circuit is usually set up with the help of a breadboard and a multitude of jumper wires. Once the circuit is working like intended, it can be simplified using a printed circuit board (PCB). Therefore, most electrical devices incorporate a PCB to save space and speed up the manufacturing process.

A PCB consists of an electrical insulating substrate and conductive paths. The substrate typically is made of epoxy and copper cladding is used for the conductive traces. CAD is preferably used to sketch an electrical circuit, which then is printed on the board using acid etching or milling. Multiple insulated layers can be used for the PCB, depending on the complexity of the electric circuit. Holes are drilled into the board and plated to connect the layers, where needed. On the other hand, nonplated holes may be used for mounting purposes [30].

The field of application of a PCB enlarged even more by PCB assembly. This method allows parts like pin sockets or small modules to be soldered directly onto the surface of the PCB. In general, a PCB can be ordered inexpensively and is manufactured rapidly. Mostly, the PCB assembly is also automated and saves time instead of soldering on all parts by hand.

3. Methods

The design of the material testing machine was created by comparing and analyzing already existing models of universal testing machines. The universal testing machine *MT-01*, which was created by Dr. Pahr Ingenieurs e.U. (Pfaffstätten, Austria), was taken as the main inspiration for the basic design. The designed was adapted in such a way, that it can bear more load and is easier to operate.

The *MT-02* was built at the TU Wien, using the tools and machines available there. The only exception is the PCB, which was ordered and manufactured off-site. All used software is open-source to allow everyone to replicate the machine. Therefore, the main used programs are all open-source as well: *FreeCAD* for CAD, *KiCad* for the PCB design, *PrusaSlicer* for 3D printing, *Arduino IDE* for microcontroller programming and *PuTTY* to export the serial data to a text file.

Eventually, the accuracy of the machine was validated by performing a tensile test on the *MT-02* as well as on a *ZwickRoell* universal testing machine. The results of the *MT-02* were compared to the ones from the *ZwickRoell* testing machine. Assumptions about the precision and accuracy of the stress and the strain data were made by analyzing the results.

3.1. Design

The design was chosen to be simple and easy to use. This allows the machine to meet the requirements of being light weight, cheap and easy to extend, while still withstanding loads up to some kN.

The frame is based on 40 mm x 80 mm aluminum profiles, on which aluminum mounts and 3D printed PETG parts are attached to with M8 screws and slot nuts. Figure 14 shows the whole assembly of the machine as a CAD model. Two NEMA 17 stepper motors are used to move the crosshead. These motors include each a gearbox with a gear ratio of 19.203:1 and are operated via two *DM542T* stepper drivers. Two ball screw sets (SFU 1605) with 0.5 m long spindles lead the vertical movement of the crosshead. The measurement of the load is conducted with the help of a load cell, which is designed for a maximal load of 5 kN.

3.1.1. Frame

The frame of the machine is made of aluminum profiles groove 8 I-type lightweight anodized black with a cross section of 40 mm width and 80 mm height. The length of the aluminum profile varies between 300 mm and 590 mm. Figure 15 shows the CAD model of the frame of the machine.

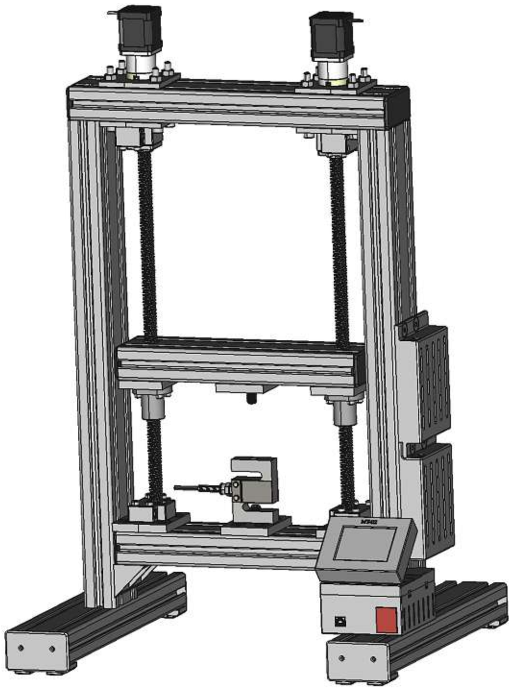

Figure 14.: *CAD model of the material testing machine*

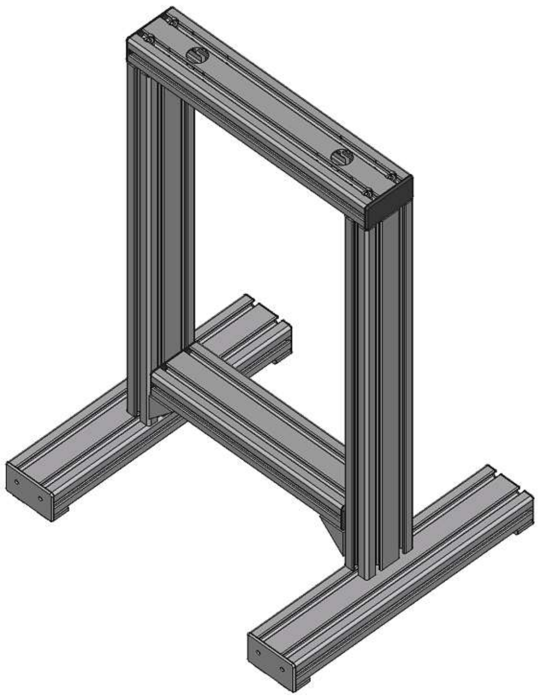

Figure 15.: *CAD model of the frame*

The profiles were modified with bores and threaded holes. This facilitates the assembly of the whole frame. The bores were made with a milling machine and the threaded holes by hand. Burrs, which resulted from the modifications, were removed with hand files. The technical drawings of the aluminum profiles are displayed in Figure 16.

Crosshead

The aluminum profile of the crosshead has a length of 300 mm and is modified with two bores with a diameter of 20 mm, to allow the spindle to pass through.

Feet

Two 8.5 mm bores are added to each one of both 400 mm long aluminum profiles. These bores are used to attach the feet to the columns. They are located with a distance of 20 mm to both sides of the horizontal axis of symmetry of the feet and placed centrally in the groove of the profile. A 12.25 mm deep bore with a diameter of 13.5 mm is added to the bottom side of the foot. This allows the head of the bolt to rest flat on the top of the nut core.

Top Beam

The couplers are lying within the top beam, which has a length of 400 mm. Therefore, two bores with a diameter of 27.5 mm are needed to enable full rotation of the coupler with enough clearance. Eight bores with a diameter of 8.5 mm are added to the top beam. This allows the fixation of the stepper motor mounts and the fixed bearing mounts. Two bores with a diameter of 8.5 mm at both ends of the top beam allow M8 screws to fit through the aluminum profile. These bores lie within the grooves. So a bigger bore with a depth of 13.5 mm is needed on the top side to allow the M8 screws to lie flat on the nut core of the aluminum profile.

Columns

On both ends of the columns two M8 threaded holes are made in the center holes of the profiles with a depth of 35 mm. The dimensions of the center holes deviate from their technical drawings due to inaccuracy of the manufacturing. Therefore, the holes with a diameter down to 6.6 mm are cut with a 6.8 mm *Makita* hand drill to get rid of the additional material. This allows the three stage bottoming tap set, which is used with a hand drill, to precisely cut the M8 thread into the bore.

Bottom Beam

The aluminum profile of the bottom beam with a length of 320 mm is not modified in any way.

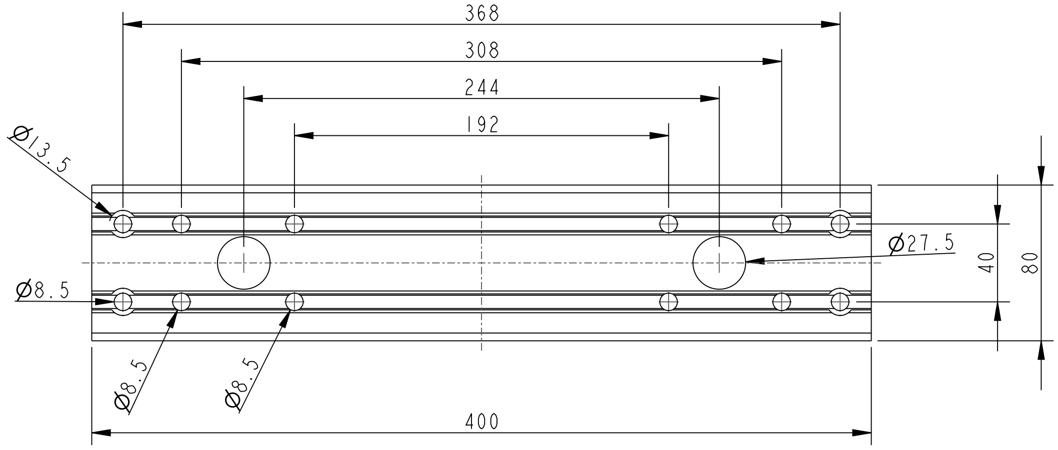

(a) *Top beam*

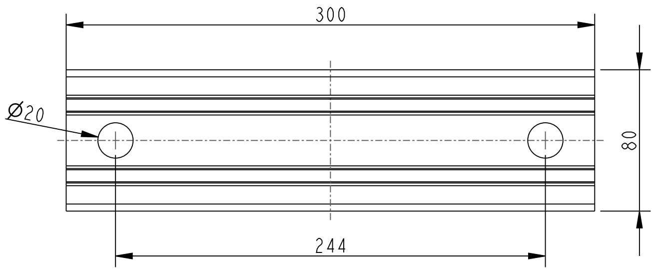

(b) *Crosshead*

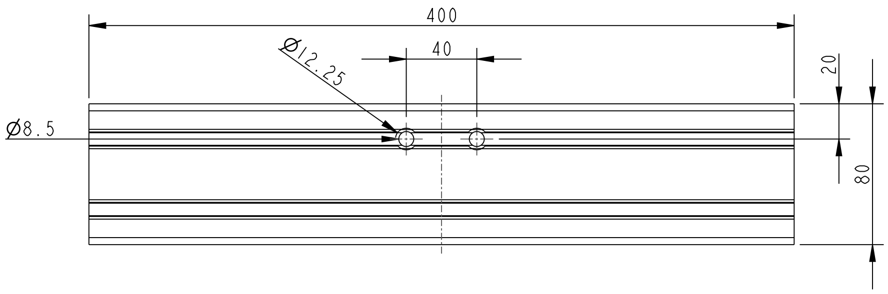

(c) *Feet*

Figure 16.: *Technical drawings of the modified aluminum profiles (unit: mm)*

3.1.2. Mounts

Mounts are designed to fix the bearings, the motors, and the ball screw nuts to the frame. The mounts are fabricated out of the aluminum alloy AW 6060. Their design was first created with *FreeCAD* and 3D printed to test the functionality. Figure 17 shows the technical drawings of the five different mounts.

The material was bought as a flat bar with the right thickness (of 6 mm and 10 mm) and width (of 70 mm and 80 mm, respectively). A band saw was used to cut ten pieces altogether of the right length from both flat bars. Each part was clamped in a vise with jaws protecting their surface and filed using two different sizes of files and sand paper (Figure 18). This procedure ensures smooth edges without any burrs.

A milling machine (Figure 19) was used to drill the holes and threads into the parts. Each mount had to be manufactured twice. So two parts were clamped together into the milling machine (Figure 20) to speed up the process. Only for countersinking, the part, which was on the bottom, had to be clamped individually after the drilling. As shown in Figure 20, a piece of wood was used to compensate for any dissimilarity between the width of both parts. While using this method, special attention has to be made concerning the coordinate system of the milling machine. It is important to set the origin of the coordinate system based on the edge without the wood to ensure high precision. The removals of the burrs were done either with the milling machine or by hand with a hand vice. The final mounts are displayed in Figure 21.

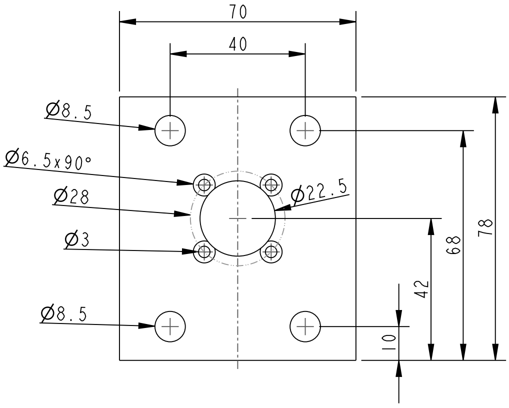

(a) *Stepper motor mount*

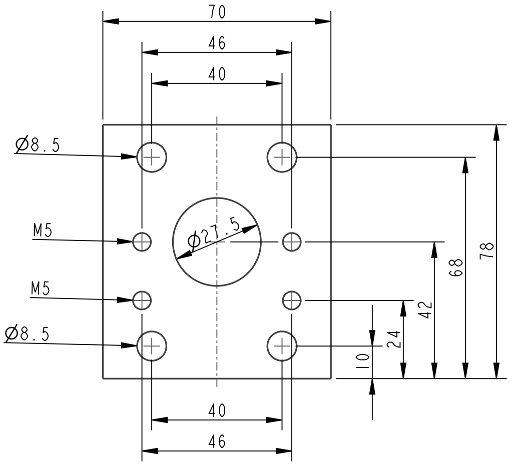

(b) *Fixed bearing mount*

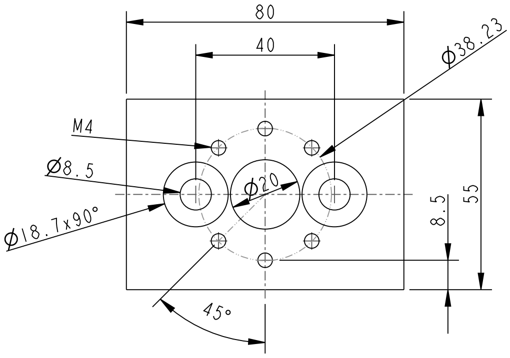

(c) *Nut mount*

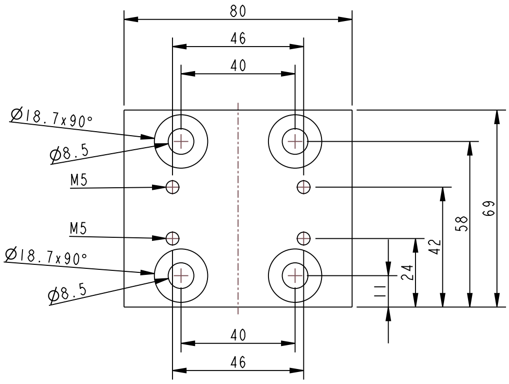

(d) *Floating bearing mount*

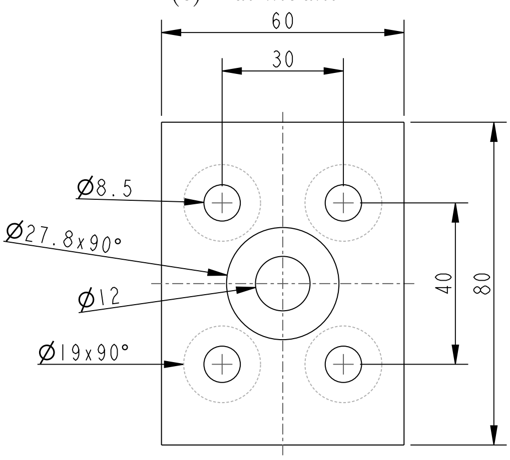

(e) *Load cell mount*

Figure 17.: *Technical drawing of the five different mounts (unit: mm)*

Figure 18.: *Aluminum alloy part clamped using special jaws protecting the surface from indentation of the vise and sand paper as well as files*

Figure 19.: *Milling machine with the clamped top beam*

Figure 20.: *Aluminum alloy parts clamped in the milling-machine with a piece of wood to compensate for dissimilarities*

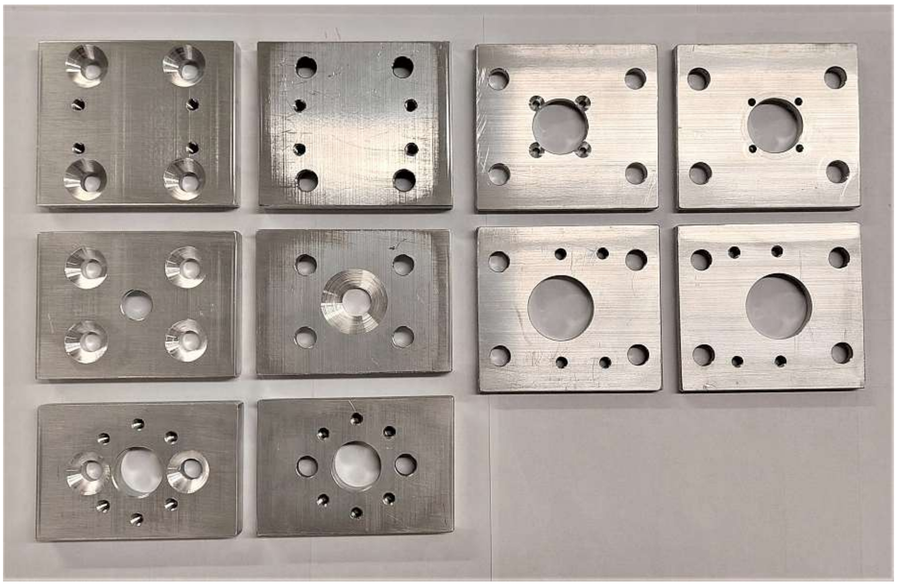

Figure 21.: *Mounts made of AW 6060. The two columns on the left have a thickness of 6 mm and the two on the right of 10 mm. As each part is made twice, the top as well as the bottom side of each mount are displayed next to each other.*

Load Cell Mount

The load cell mount is designed in a sturdy and practical way to reduce the influence of the machine parts on the result while testing. Therefore, a thickness of 10 mm was chosen. The distances of the bores with a diameter of 8.5 mm are located accordingly to the spacing of the aluminum profile slots. These bores are used to fixate the mounts to the aluminum profiles with the help of M8 screws and slot nuts. For the design of the mount the dimensions of the load cell were taken into account to enable handy mounting. The countersinks ensure that the M8 screws do not touch the load cell after assembly. The bore with a diameter of 12 mm in the middle matches the thread size of the load cell and is countersunk to avoid any touching and scratching of the M12 screw with the beam to which this mount is attached. The width (60 mm) was chosen to enable enough spacing between the bores and the edges of the part. Initially the length was designed to be 70 mm, for the part to be located with some space to the edges of the bottom beam of the machine for economical reasons. However, due to the unavailability of an aluminum alloy flat bar with the desired dimensions, the length was changed to the next larger size of 80 mm. For the sake of simplicity and efficiency this dimension was transferred to all mounts with a thickness of 10 mm.

Nut Mount

The bores with a diameter of 8.5 mm in the nut mount have a distance of 40 mm to each other for the M8 screws to fit into the parallel aluminum profile slots. The bore in the middle with the diameter of 20 mm allows the spindle with a diameter of 16 mm to pass through with enough clearance. Six M5 threaded holes are placed according to the hole dimensions of the nut. This allows the fixation of the nut to the mount. Enough material is needed for the M5 screw to grip into. Therefore, the thickness was chosen to be 10 mm. The width of 55 mm was chosen to have enough space from the bores to the edges of the mount as well as to the edge of the crosshead.

Floating Bearing Mount

The thickness of the floating bearing mount is chosen to be 10 mm. Like the other mounts with this thickness, the length is designed to be 80 mm. The width on the one hand allows the edge to coincide with the side columns of the machine and on the other hand ensures that the center of the bearing lies on the same axis as the one of the spindle. The M5 threaded bores are placed according to the dimensions of the bearing.

Stepper Motor Mount

Initially the mount for the stepper motor was planned with a thickness of 7 mm but as only an even number for the thickness of the aluminum alloy flat bar was available, the thickness was reduced to 6 mm. It is crucial to have enough clearance between the coupler and the mount. So, a PETG part, the stepper motor spacer, with a thickness of 1 mm has to be placed between the aluminum alloy mount and the top beam. This spacer is used to compensate for the one missing millimeter of the stepper motor mount. The bores with the diameter of 8.5 mm are not countersunk. In contrast to the mounts with the higher thicknesses, they are not used for screws with slot nuts but for bolts with nuts. This means that the top beam and the fixed bearing mounts have the same bores with a diameter of 8.5 mm, where an M8 bolt can be put through and fixed on top of the stepper motor mount with nuts. A width of 70 mm, which is slightly smaller than the width of the top beam, is chosen for this mount. The length is set to 78 mm. The diameter of the bore for the shaft of the stepper motor was decided to be 22.5 mm. This guarantees that the top part of the stepper motor with a diameter of 22 mm fits. Four bores with a diameter of 3 mm and countersinks are made around the bore with the diameter of 22.5 mm. These bores are used to screw the motor to the mount.

Fixed Bearing Mount

The fixed bearing mount resembles the stepper motor mount to a high extent. This ensures that the location of the bores with a diameter of 8.5 mm is identical.

Four M5 threaded bores are made according to the dimensions of the fixed bearing. Furthermore, the bore in the middle has a diameter of 27.5 mm to fit the coupler. The 3D printed fixed bearing spacer is used to ensure enough clearance for the coupler to rotate freely, without touching the stepper motor mount.

3.1.3. Additive Manufacturing

Two fused deposition modeling (FDM) *Prusa* 3D printers, the *Original Prusa MINI+* and the *Original Prusa i3 MK3*, were used to produce the parts out of PETG and thermoplastic polyurethane (TPU). The parts were designed with *FreeCAD*, exported as *step* files and sliced with *PrusaSlicer*. Principally the *Original Prusa MINI+* printer was used for parts made of PETG, while for bigger parts or parts made of TPU (i. e. the dampers for the end caps) the *Original Prusa i3 MK3* printer was utilized.

The printed parts are the following, where every part with exception of the dampers, was fabricated out of PETG:

- End caps
- Spacing for stepper motor mount
- Spacing for BK12 mount
- Cable caps
- Housing
- Spacing cylinders for the PCB
- Dampers for end caps

The geometry of the end caps was adapted from the precursor machine and modified to fit the 40 mm x 80 mm aluminum profiles (instead of the 40 mm x 40 mm aluminum profiles). The dampers and cable caps were adopted from the precursor without any modification.

The spacing parts for the stepper motor mount and the fixed bearing mount were 3D printed with a thickness of 1 mm. Their geometry is adapted from the mounts themselves but simplified. Their technical drawings are displayed in Figure 22.

3.1.4. Stepper Driver

The digital stepper driver *DM542T* ensures a smooth current wave form. Additionally, it is capable of feeding the stepper motors with enough power to operate with a crosshead speed up to at least 520 mm min^{-1}. Furthermore, the digital stepper driver is able to generate enough current, while not producing excessive heat.

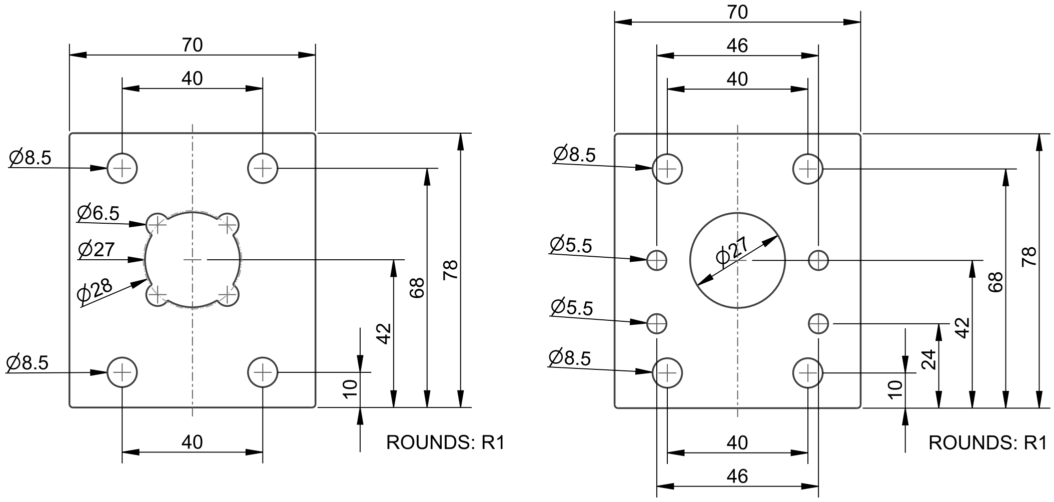

(a) *Spacer for the stepper motor mount (unit: mm)*

(b) *Spacer for the fixed bearing mount (unit: mm)*

Figure 22.: *Dimensions of the distances used for the mounts of the stepper motor and the fixed bearing. Their thickness is set to 1 mm.*

3.1.5. Design Calculations

Maximum Force

For a NEMA 17 motor with a holding torque, M, of 0.52 N m [17] and a microstep resolution of an 8$^{\text{th}}$ step, the actual holding torque without any gearbox, M_{MS}, is 0.0975 N m. With a gearbox with a gear ratio, N, of 19.203:1 [17], an efficiency of the nut, η_{Nut}, of 90 %, an efficiency of the stepper motor, η_{Stepper}, of 80 % [17], and a linear rail with a lead, L, of 5 mm [31] the maximum axial force is estimated by:

$$\begin{aligned} F_{\text{ax}} &= \frac{M_{\text{MS}} \cdot 2\pi \cdot N \cdot \eta_{\text{Nut}} \cdot \eta_{\text{Stepper}}}{L} \\ &= \frac{0.0975\,\text{N m} \cdot 2\pi \cdot \left(19 + \frac{38}{187}\right) \cdot 0.90 \cdot 0.80}{0.005\,\text{m}} = 1.694\,\text{kN} \end{aligned} \tag{8}$$

When two identical motors with identical gearboxes are used to drive the machine, the calculated value of the axial force in Equation 8 is doubled to obtain a total axial force of $F_{\text{ax}} = 3.388\,\text{kN}$.

Crosshead speed

The speed of the crosshead is directly linked to the rotational speed of the motor. This rotational speed, which is commonly given in revolutions per minute (RPM), is controlled by the frequency of rising edges in the signal at the pulse pin of the stepper driver. Therefore, wider pulse widths result in slower rotations of the motor shaft. This leads to lower crosshead speed.

If the widths of the high and low signals are set to be equal, the steps per second, SPS, are determined dependent on the desired crosshead speed, CHS, as follows:

$$SPS = \frac{SPR \cdot MS}{L} \cdot CHS \tag{9}$$

with the steps per revolution, SPR, representing the number of steps needed for a full rotation of the shaft of the stepper motor without microstepping. MS stands fot the number of microsteps (e.g. 8 for the use of a microstep resolution of 8$^{\text{th}}$ step) and L represents the distance the nut of the spindle moves with one full revolution. This value is known as the lead of a spindle and is stated in the datasheet of the ball screw. The steps per revolution without microstepping are calculated as follows:

$$\begin{aligned} SPR &= \frac{360°}{\alpha} \cdot N \\ &= \frac{360°}{1.8°} \cdot \left(19 + \frac{38}{187}\right) = 3840.64. \end{aligned} \tag{10}$$

The step angle without the gearbox, α, and the gear ratio, N, can be obtained from the datasheet of the stepper motor [17].

The reciprocal value of the number of steps per second has to be formed and multiplied by 10^6 to convert the value from s to µs. This value then describes the pulse width (or pulse delay), PW, in µs. One step represents two pulses (high and low). So the whole expression has to be divided by two to get the pulse width. This leads to:

$$PW = \frac{10^6}{2 \cdot SPS}. \tag{11}$$

The stepper driver *DM542T*, which was used to control the stepper motors for the *MT-02*, has a minimal pulse width of 2.5 µm [20]. Using this minimal pulse width as well as Equation 9, Equation 10, and Equation 11, the potential maximal crosshead speed is calculated to be 19 500 mm min^{-1}. However, other components in the assembly, like the stepper motor, can reduce the actual maximal crosshead speed drastically.

In the final design of the *MT-02*, the maximal crosshead speed is chosen to be 450 mm min^{-1}. A very unpleasant high-pitched sound is audible at higher speeds.

3.1.6. Circuit Diagram

In order to come up with the final schematic of the electrical circuit, all modules were tested individually, then together on a breadboard. A PCB was manufactured to simplify the whole setup. It was designed such that it can be used as a shield for the *Arduino Mega 2560*.

Some ideas came up during the process of designing the electrical circuit, which eventually resulted in a dead end. Those discarded design ideas are described in section A.2.

Electrical Circuit

The *Arduino* microcontroller is used as the base, where the PCB and the shield for the TFT LCD are stacked on, respectively. With a ribbon cable the TFT LCD is then connected to its shield. The *HX711* analog-to-digital converter and the 24 V to 5 V DC/DC converter are directly soldered onto the PCB. The load cell and the digital stepper drivers are linked to the PCB with the help of JST connectors. The power jack and the rocker switch are connected to the PCB via screw terminals. The same connection is used for the stepper motors to be wired to the digital stepper drivers. Figure 23 shows the pictorial diagram of the whole electrical circuit drawn with the open-source software *fritzing*. Pictures of the PCB as well as of the stepper drivers were imported to the vector graphics software *Inkscape*, converted to vector graphics and exported as SVG files. These were then imported to the *Fritzing Parts Editor*, where the specific locations of the pins on the graphics could be defined, to create new parts in *fritzing*. For the sake of clarity, the 24 V to 5 V converter is represented as a much bigger module in the schematic of the circuit diagram. Actually, a small module is used and directly soldered onto the PCB.

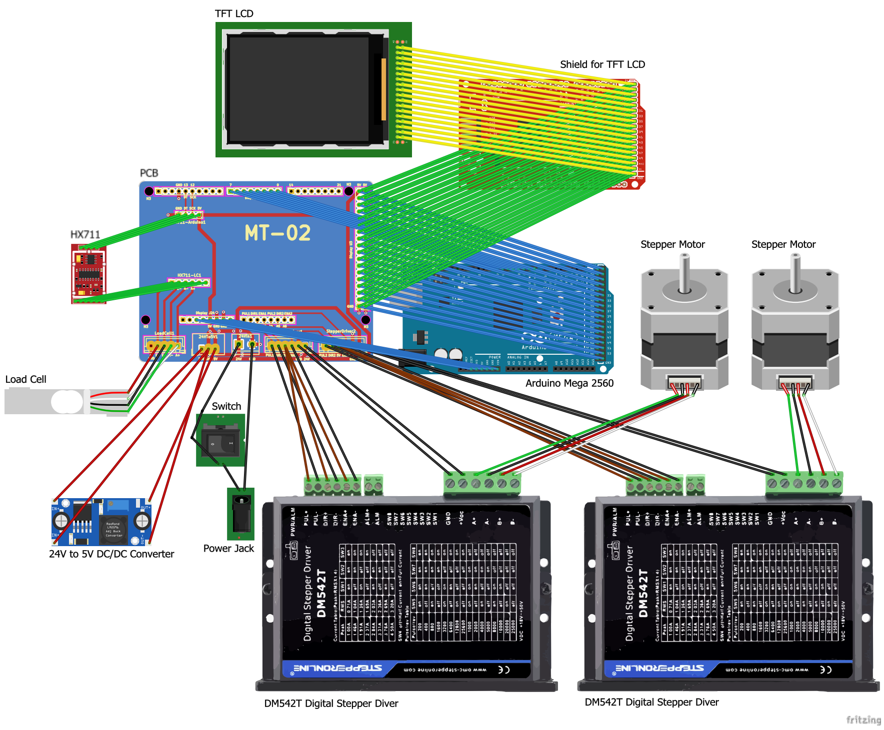

Figure 23.: *Circuit diagram of the MT-02*

PCB

A PCB was designed as a shield for the *Arduino Mega 2560*. The use of stacking headers allows the shield for the TFT LCD to be stacked on top of the PCB. The digital version of the two layered PCB, which was designed in *KiCad*, is shown in Figure 24.

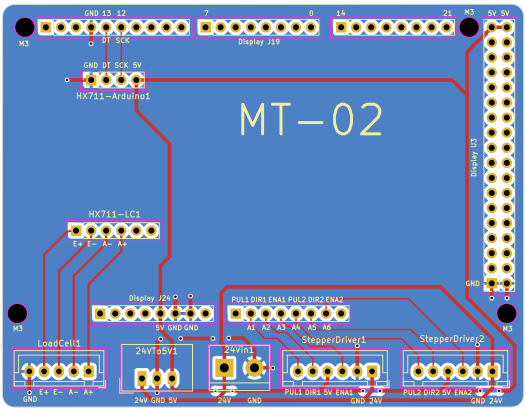

Figure 24.: *Schematic view of the top layer of the PCB as designed with KiCad*

The following files were exported from *KiCad*. These were then uploaded to *JLCPCB*, where the PCB was ordered from:

- NPTH.drl
- PTH.drl
- B_Cu.gbr
- B_Mask.gbr
- Edge_Cuts.gbr
- F_Cu.gbr
- F_Mask.gbr
- F_Silkscreen.gbr
- NPTH-drl_map.drl
- PTH-drl_map.drl

Figure 25 shows the PCB as delivered by *JLCPCB* with all required parts in an exploded representation. Figure 26 depicts the PCB assembly. All parts were soldered on by hand.

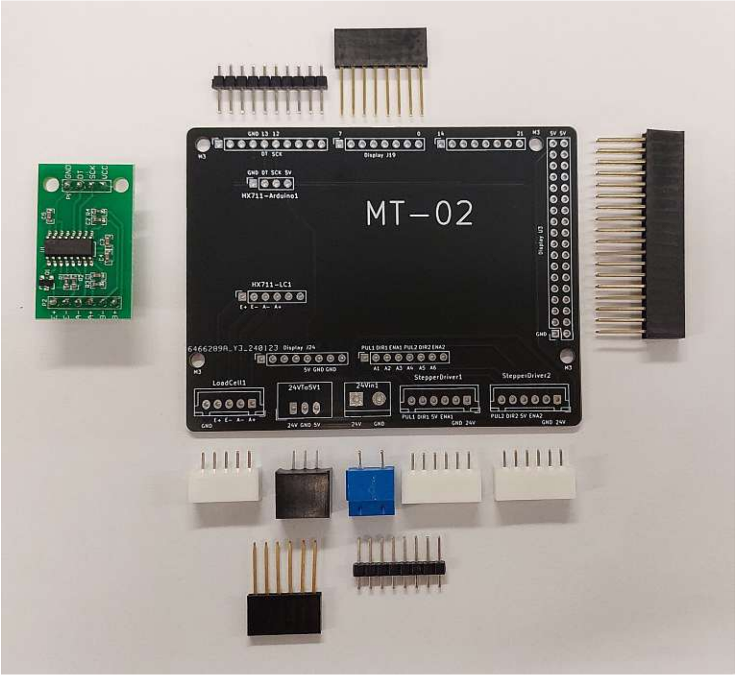

Figure 25.: *Exploded view of the PCB and all required pins, sockets, the HX711 module and the DC/DC converter*

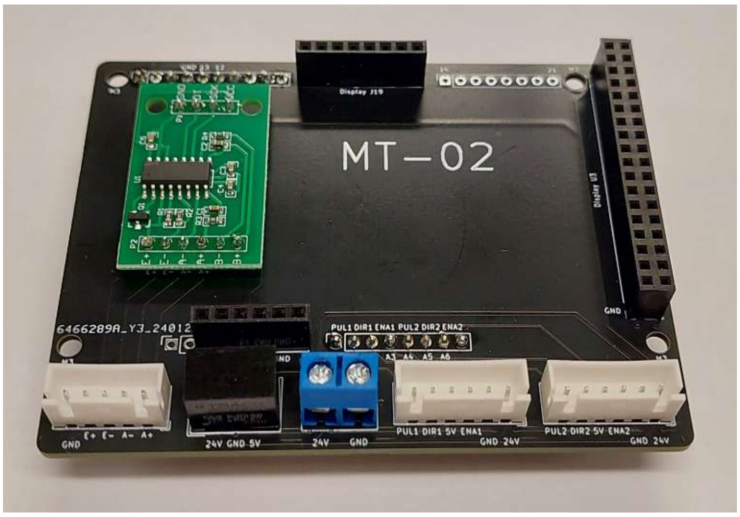

Figure 26.: *Assembled PCB*

3.2. Assembly

In this section the process of assembly is described. All the materials, which are needed to build the *MT-02* are listed in section A.1. Figure 27 shows some steps of the assembly process.

3.2.1. Top Beam

The assembly process of the frame starts with attaching both columns (i. e. the aluminum profiles with a length of 590 mm) to the top beam (i. e. the aluminum profile with a length of 400 mm) using four M8x45 mm hex screws (Figure 27a). It is important to ensure a parallel alignment of the columns. This is done by precisely lining up the ends of the columns with the faces of the top beam.

3.2.2. Crosshead

Both nut mounts are screwed on the bottom of the crosshead (i. e. the aluminum profile with a length of 300 mm) aligning the bores via four M8x20 mm countersunk screws and four M8 slot nuts (Figure 27b). End caps are added and the nuts of both ball screws are each attached to one of the nut mounts with six M5x20 mm hex screws for each one. Putting lubricant on the top end of the spindle facilitates its insertion into the fixed bearing. Thus, the nut of the fixed bearing can be screwed on and tightened using a 2 mm hex key. Both fixed bearings are attached to their mounts (Figure 27c) by using eight M5x35 mm hex screws.

3.2.3. Stepper Motors

The stepper motors are fixed to the stepper motor mounts by four M3x10 mm countersunk screws each. The connection between the stepper motor shaft and the spindle is achieved by tightening a coupler with a diameter of 25 mm and a length of 40 mm to the stepper motor shaft. Thereby it is necessary to make sure that the screws on the other side of the coupler are loosened. The stepper motor mount and the fixed bearing mount with their 3D printed spacers are then screwed on the top beam with eight M8x70 mm hex screw, eight washers, eight nuts, and eight cover caps in total (Figure 27d). It is important to assure a centered position. This allows the coupler to rotate freely within the bore of the top beam. Otherwise the screws in the coupler could touch the top beam, abrading the screws.

3.2.4. Bottom Beam

Both floating bearing mounts are attached to the bottom beam (i. e. the aluminum profile with a length of 320 mm) using eight M8x20 mm countersunk screws and eight M8 slot nuts. Four corner brackets are tightened to the bottom beam with four M8x16 mm raised countersunk screws and four slot nuts. This prepares the bottom beam for the attachment to the columns. The bottom end of the spindle is put

(a) *Frame with the crosshead and both spindles fixed to their mounts*

(b) *Crosshead with nut mounts, screws, hex key, and slot nuts*

(c) *Spindle attached to the fixed bearing, which is attached to its mount, and the ball screw nut attached to the crosshead*

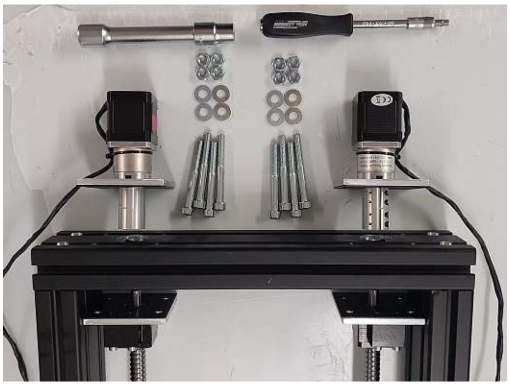

(d) *Top beam with the stepper motors, the fixed bearings, the couplers, the mounts, the spacers (black), and all needed screws and tools for the fixation*

(e) *Bottom beam with the screws and hex key needed to attach the floating bearing to the bottom beam via its mount*

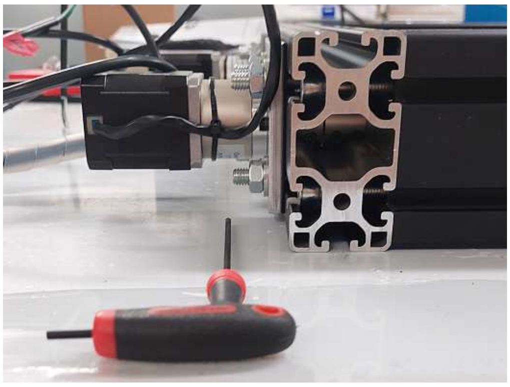

(f) *Side view of the top beam with the long hex key, which is needed to tighten the screws of the already inserted coupler*

Figure 27.: *Pictures of the assembly process*

into the floating bearing and fixated with a circlip to prevent slipping. The floating bearing can then be screwed to the floating bearing mount via four M5x30 mm hex screws for each side (Figure 27e). It should be asserted that both ball screw nuts are at the same height, while inserting the top shaft of the spindle into the coupler. A 2.5 mm hex key, equipped with a long arm of at least 10 mm and a ball point, is put through the lateral opening of the top beam (Figure 27f). Thereby, both bottom screws of the coupler can be tightened. Ideally the electronics are already connected to the steppers, allowing the coupler to rotate until it reaches the perfect position for the hex key to tighten the screws. End caps are then used to cover these openings. The bottom beam can be held in the correct position by screwing the corner brackets to the columns using four M8x16 mm raised countersunk screws and four slot nuts.

3.2.5. Feet

Four M8x45 mm hex screws are used to attach the feet (i. e. the aluminum profiles with a length of 400 mm) to the rest of the frame. The 3D printed end caps are then secured to the feet using drywall screws. 3D printed dampers, made of flexible TPU, ensure that the machine remains stable, even on rough surfaces.

3.2.6. Load Cell

On the top of the bottom beam as well as on the bottom of the crossbeam the load cell mounts are attached with eight M8x20 mm countersunk screws and eight M8 slot nuts. The load cell itself is fixated to the load cell mount with an M12x35 mm countersunk screw. Ideally, the grips used for the testing are equipped with M12 threads. This way, the bottom grip can be screwed to the load cell with a stud bolt and the top grip attached to the top load cell mount with an M12 countersunk screw.

3.2.7. Housing

The stepper driver housing is 3D printed and attached to the right column, when facing the machine from the front, with four M8x20 mm countersunk screws and four slot nuts. Two M4x10 mm slotted screws are screwed into the respective threaded bore of the stepper driver housing to hold the stepper drivers in position. The *Arduino* with the PCB and the TFT LCD shield are fixed to the bottom *Arduino* housing using two M3x20 mm and two M3x35 mm slotted screws. The bottom *Arduino* housing itself is attached to the anterior part of the right foot with two M8x20 mm countersunk screws and two slot nuts. The top *Arduino* housing is held on the bottom one with the help of a snap fit locking mechanism. The display is held in an inclined position via snap fit on the top *Arduino* housing for the sake of ergonomic operation. The housing for the display is 3D printed and attached to the display with four M3x6 mm slotted screws.

3.3. Software

The *Arduino* IDE is used for uploading the code to the microcontroller as well as for using the serial port. The library *HX711_ADC* by Olav Kallhovd is utilized for the load cell. The libraries *UTFT* [32] and *URTouch* [33] from *Rinky-Dink Electronics* are applied to control the touch display. The *Arduino* library *EEPROM* is needed to store the calibration factor in the non-volatile memory.

The *UTFT* library from *Rinky-Dink Electronics* includes the tool *ImageConverter565*. This application allows the conversion from a JPEG image to a bitmap, which makes it easier to print icons on the display. This was used for the home icon as well as for the up, down, and back pointing arrows, which were designed and exported as JPEG images with the GNU image manipulation program (GIMP).

The first screen after powering on the machine is the home screen. It shows a menu with all basic functions, which are further described in the following sections. Pictures of the screen are depicted in Figure 28.

3.3.1. Home Screen

A home screen with three main buttons appears, when powering on the machine. The functions *Manual testing*, *Travel mode* and *Calibration* can be chosen by pressing one of the main buttons. On the bottom right a button with an arrow allows to switch to the second page of the home screen, where by clicking on the *Stepper ON/OFF* button, the steppers can be powered on or off.

3.3.2. Manual Testing

Testing with a speed between $0.5\,\mathrm{mm\,min^{-1}}$ and $6\,\mathrm{mm\,min^{-1}}$ can be performed in the manual testing mode. The speed can be set manually with up to two decimal places. Taring can be performed and the crosshead can be controlled to move up or down. Detailed information including time, displacement, and force can be extracted using the serial port during the test. The current force is also printed on the TFT LCD screen. This allows the machine to be used without a spare computer. A test is terminated by releasing either the button, which moves the crosshead up, or by the one moving it down. The maximum measured load is printed on the TFT LCD screen after a test.

The *Arduino* code, which controls the movement of the stepper motors as well as the recording and printing of the test data, is displayed in Listing 3.1. The function `measureAndMove` performs a step with a pulse delay calculated based on the defined crosshead speed. After checking if new data from the load cell are available and the print interval is exceeded, the measurement data are calculated and printed to the serial monitor as well as to the TFT LCD screen. The print interval is based on the measurement frequency, which is set to 5 Hz. A safety factor concerning the load is included. The current load is constantly compared to the maximum permissible load. If the value is exceeded, the measurement is interrupted.

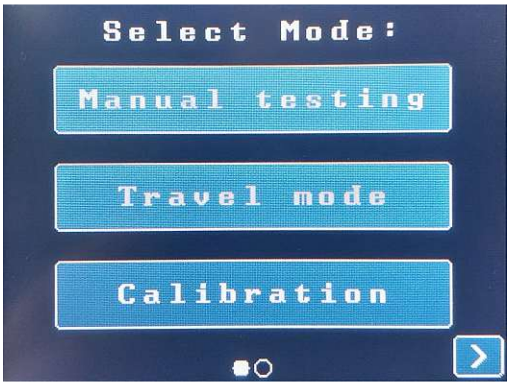

(a) *Home screen*

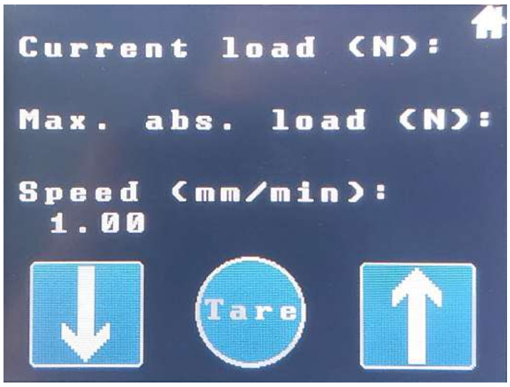

(b) *Manual testing mode*

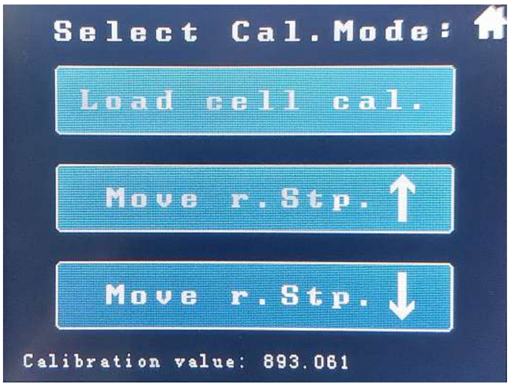

(c) *Calibration mode*

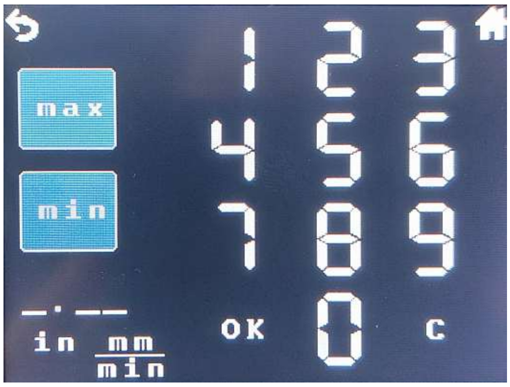

(d) *Measurement speed settings*

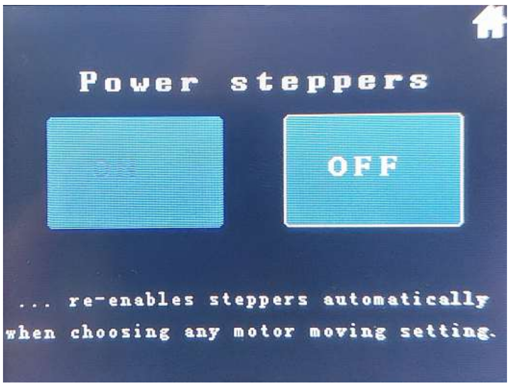

(e) *Power on/off the stepper motors*

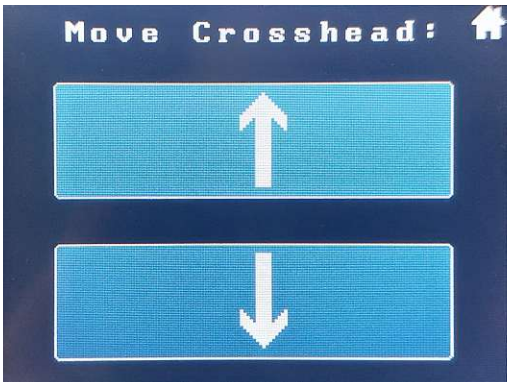

(f) *Travel mode*

Figure 28.: *Pictures of the TFT LCD screen*

An adequate error message is printed to the serial monitor and displayed on the TFT LCD screen with the magnitude of the load. This safety mechanism is further specified subsection 3.4.2.

Listing 3.1: *Code controlling the movement of the stepper motors and acquiring the test data*

```
void measureAndMove(int x1, int y1, int x2, int y2) {
  pulseDelay = calcPulseDelay();
  Serial.print("Measurement␣speed␣(mm/min):␣");
  Serial.println(crossheadSpeedMMPerMin);
  maxLoadCellValue = 0;
  myGLCD.setColor(255, 0, 0); // red
  myGLCD.drawRoundRect (x1, y1, x2, y2);
  myGLCD.setBackColor(0,0,0);
  myGLCD.setColor(255, 255, 255);
  myGLCD.setFont(BigFont);
  enableStepper(STEPPER_1_AND_2);
  // set direction
  digitalWrite(STEPPER_1_DIR_PIN, direction);
  digitalWrite(STEPPER_2_DIR_PIN, direction);
  delayMicroseconds(5); // see driver datasheet
  pulseCount = 0;
  startTime = millis();
  Serial.println("START␣Measurement");
  Serial.println("Time(s);Travel(mm);Force(N)");
  while (myTouch.dataAvailable()){ // as long as touched
    // perform step
    digitalWrite(STEPPER_1_PUL_PIN, HIGH);
    digitalWrite(STEPPER_2_PUL_PIN, HIGH);
    delayMicroseconds(pulseDelay);
    digitalWrite(STEPPER_1_PUL_PIN, LOW);
    digitalWrite(STEPPER_2_PUL_PIN, LOW);
    pulseCount++;
    // check if HX711 is ready
    boolean newDataReady = false;
    if (loadCell.update()) newDataReady = true;
    if (millis() > readOutTime + serialPrintInterval) {
      if (loadCell.update()) newDataReady = true;
      if (newDataReady) {
        // seconds passed since start of measuring (float
          )
        timeData = (millis()-startTime)/1000.0;
        travelData = float(pulseCount/float(
          stepsPerRevolutionFull*microsteps))*pitch;
```

```
        loadCellData = abs(loadCell.getData());
        if(loadCellData > maxLoadCellValue){
          maxLoadCellValue = loadCellData;
        }
        // for safety
        if(loadCellData > maxLoadValue){
          loadCell.update();
          loadCellData = abs(loadCell.getData());
          if(loadCellData > maxLoadValue && direction == LOW){ // DOWN
            Serial.println("Maximal␣compression␣load␣value␣exceeded!");
            maxLoadExceededScreen();
            getLoadCellData(2); // sec time delay
            drawManualTestScreen();
            break;
          }
          if(loadCellData < -maxLoadValue && direction == HIGH ){ // UP
            Serial.println("Maximal␣tensile␣load␣value␣exceeded!");
            maxLoadExceededScreen();
            getLoadCellData(2); // sec time delay
            drawManualTestScreen();
            break;
          }
        }
        Serial.print(timeData,3);
        Serial.print(";");
        Serial.print(travelData,5);
        Serial.print(";");
        Serial.println(loadCellData,3);
        // print on screen
        myGLCD.printNumF(loadCellData, 2, 30, 20+20); // num, dec, x, y
        readOutTime = millis();
      }
    }
    delayMicroseconds(pulseDelay);
  }
  pulseCount=0;
  Serial.println("END␣Measurement");
  drawManualTestScreen();
}
```

3.3.3. Load Cell Calibration

A reference weight is needed for the calibration of the load cell. The button *Load Cell Cal.* in the *calibration* mode has to be pressed once to perform the calibration. This will show a screen saying that further information is given in the serial monitor. The calibration has to be done by connecting a computer to the machine via USB and by using the serial monitor. This ensures that no misuse or accidental pressing of the *Load Cell Cal.* button can lead to an unwanted change of the calibration value during a series of tests. At the end of the calibration, the user can decide whether the new calibration factor should only be used as long as the machine stays powered on or saved to the electrically erasable programmable read-only memory (EEPROM). Saving the calibration value to the EEPROM ensures that it will be used for future tests, even if the machine was powered off in between.

3.3.4. Realignment of the Crosshead

One motor can be controlled independently from the other one. This allows to compensate for any missed steps of the stepper motors and consequently to the deviation of the crosshead from the horizontal axis. Realigning the crosshead can be done by pressing and holding the respective button, which either moves the right stepper, as observed from the front, up or down until the crosshead again reaches the horizontal position.

3.3.5. Power On/Off the Stepper Motors

The stepper motors are drawing current even if they are not moving. Therefore, they can be powered on and off to lower the power consumption and the noise. This preference can be set on the second page of the home screen by pressing the respective *ON* or *OFF* button. The current state is indicated by a colored border and font. Powering off the steppers is only intended for the reasons that are mentioned above. This is why the stepper motors will power on again automatically if any mode that moves the crosshead (*measure*, *travel* or *calibration*) is selected.

3.4. Safety Mechanisms

Safety is an important factor for all devices operated by humans, especially in teaching or during demonstration. So, multiple independent safety mechanisms are integrated in the testing machine. These mechanisms are further explained in the following subsections.

3.4.1. Only Moving While the Button is Pressed

The software does not include any automation concerning the movement of the crosshead. This means that the crosshead can only travel up or down while the respective button is pressed and held down. If any unwanted movement were about to happen, the operator is expected to wince and automatically cease touching the display. This immediately stops the crosshead and prevents eventual damage.

3.4.2. Stopping at Maximum Force

In *manual testing* mode, the force is measured by the load cell. Therefore, a safety query is included in each step, where the measured value is compared to a predefined force maximum. If this maximum is exceeded, the machine stops immediately. This surpassing is printed to the screen with the actual applied load as an information for the user. Furthermore, the machine can only move in the opposite direction of load application (while in *manual testing* mode) to decrease the load until it falls below the configured threshold. Every other mode than the *manual testing* mode does not take information from the load cell. Therefore, the movement of the crosshead is not restricted by the threshold in those modes.

3.4.3. Restricted Power of the Stepper Motors

If the maximum load is exceeded while using the travel mode, the stepper motors will miss steps. This is audible by knocking noises. So, at the maximum possible load, these knocking sounds will indicate the operator of the machine to stop further movement of the crosshead.

3.4.4. Tightening Torque in the Corner brackets

The point of failure can be varied by adjusting the tightening torque of the screws in the slot nuts of the corner brackets, which mount the bottom beam to the side columns of the frame. So, the bottom beam will move downwards while sparing all other parts of irreversible failure at high loads if the tightening torque is decreased.

3.5. Testing

Tensile tests on this machine as well as on a *ZwickRoell RetroLine* universal testing machine were performed to validate the results the *MT-02* yields. The results of the *MT-02* were then analyzed and compared to those of the *ZwickRoell*. The distance on the *MT-02* was recorded using the number of steps the motors are accomplishing. The universal testing machine from *ZwickRoell*, on the other hand, uses a video extensometer to track the distance between two marks on the sample. Each test series consists of five samples. All samples were produced simultaneously using the same 3D printer. This ensures the same environmental, material and printing conditions, yielding an increased accuracy for the comparison of the results.

3.5.1. Samples

Figure 29 shows the dimensions of the samples for the *MT-02*. The samples, which were tested on the *ZwickRoell* universal testing machine had the same geometry but with the ends being extended by 11 mm on each side (Figure 30). This was needed to increase the surface area for the grips to hold the samples in place. A particularly important parameter for the evaluation of the tensile test data is the gauge length, which is defined as 15 mm. The gauge length represents a length with a constant cross-sectional area in the middle of the sample.

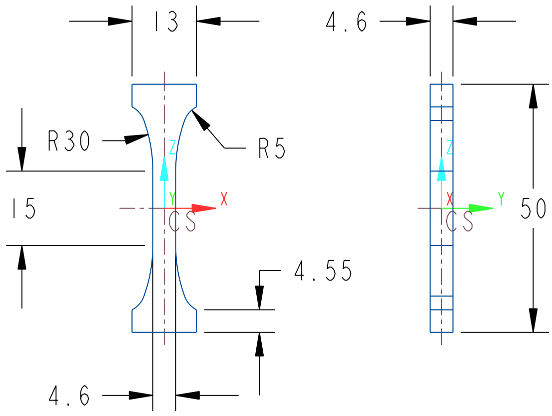

Figure 29.: *Dimensions and coordinate system of the sample for tensile testing (unit: mm)*

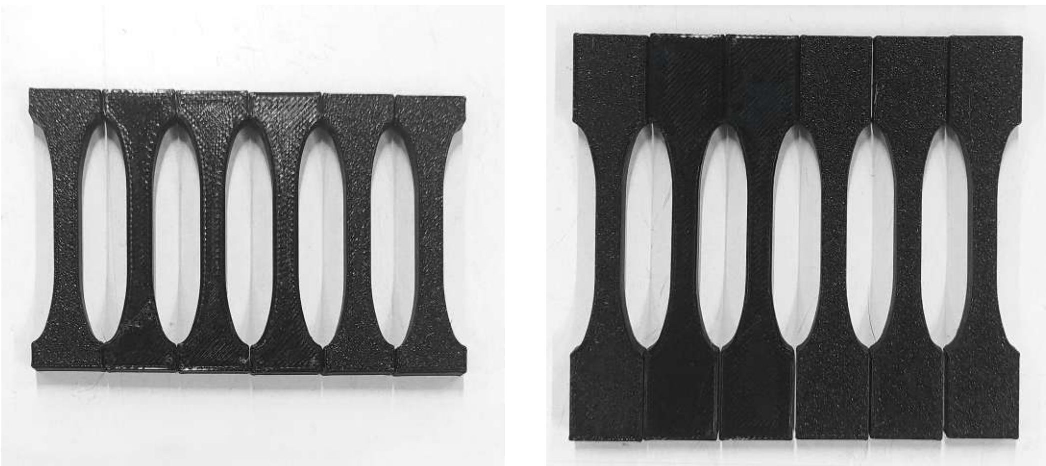

(a) *Samples for the MT-02* (b) *Samples for the ZwickRoell UTM*

Figure 30.: *3D printed PETG samples*

The material used for all samples is black PETG *from Amazon basics*. The samples are imported as *sla* files to the *PrusaSlicer*. This slicing program is used to orientate the samples on the printing sheet and to set all printing properties like the printing speed, the layer height and the heating temperature. An infill density of 100 %, a layer height of 0.2 mm and a printing speed setting of *QUALITY* in the

PrusaSlicer were used. The *QUALITY* speed setting is a preset of the *Original Prusa MINI* with a printing speed of $40\,\mathrm{mm\,s^{-1}}$ for the perimeter and $80\,\mathrm{mm\,s^{-1}}$ for the infill. The samples are printed with two contours and infill in between. As the default settings of the *PrusaSlicer* suggest, the infill lines are printed with a 45° angle. The nozzle temperature was set to 240 °C (or 230 °C for the first layer) and the bed temperature to 85 °C. The samples are oriented horizontally on the printing bed. This means that the z-axis of the sample (cyan axis in Figure 29) is aligned in parallel to the surface of the printing bed. The samples were printed a day before the testing, which ensures that they were already cooled down to room temperature before performing the test.

3.5.2. Testing Procedure

A test series consists of five tests. The dimensions of the samples are measured before testing, as the 3D printing process can lead to values deviating from the original dimensions of the CAD model. After the application of the pre-load with an amplitude of about 30 N, the distance between the clamps is increased constantly with a speed of $1\,\mathrm{mm\,min^{-1}}$. The test is finished, when a peak in the recorded load data is recorded and followed by a load drop of a certain percentage of the peak value. The data are then exported and analyzed to gain information about the material properties. The initial measured dimensions are taken into account for the calculation of the stresses and the Young's modulus, rather than those of the CAD model.

MT-02

The boundary conditions for the testing procedure with the *MT-02* are set with two clamps. This allows only movement in the vertical axis. The mount of the top clamp was not used as initially intended. The clamps, which were already manufactured for the precursor universal testing machine, are equipped with an M8 thread. An alternative mounting approach was elaborated, as the *MT-02* is designed for the attachment of clamps with M12 threads. M8 screws and washers were used to compensate for the countersunk bores. M10 nuts were used as spacers to create enough space for the head of the center screw, where the top clamp was attached. The bottom clamp was secured to the load cell with an M12 to M8 thread reduction adapter. This setup is depicted in Figure 31.

The testing was executed at a temperature of 24.2 °C. Initially, the load cell was calibrated with the help of a 0.5 kg reference weight. Before starting the actual testing procedure, the machine was connected to a laptop via USB and the software *PuTTY* was launched to export the serial data to a text file. Before inserting each sample into the clamps, the load cell was tared. This ensured that the load data were independent of the previous test.

After the application of a pre-load between 30 N and 40 N with a speed of $6\,\mathrm{mm\,min^{-1}}$, the displacement controlled tensile test was performed with a speed of

Figure 31.: *Clamps on the MT-02*

1 mm min^{-1}. The test was stopped when the sample was broken. This was indicated by a rupture or necking accompanied by a drastic decrease in force on the sample, falling below a value of 700 N after a clearly distinguishable peak in the load curve. The data of the five tests with time, displacement, and load, were acquired via the serial port and recorded with a frequency of 5 Hz. The whole procedure was performed five times. The data were then analyzed with *medtool 4.8* from Dr. Pahr Ingenieurs e.U. [34] to get information about the stress and stain as well as the Young's modulus.

ZwickRoell UTM

The testing software *testXpert III* was utilized for the test with the *ZwickRoell RetroLine* UTM with screw grips (Figure 32). The samples were prepared with adhesive white markers before starting the testing procedure. This allowed the video extensometer to detect distinct positions on the sample (Figure 33). After configuring all settings for the tensile test, the sample was tightened into the top grip. Once the program detected the markers, the force was set to zero and the bottom clamp was fastened. The machine automatically applies load to the sample with a crosshead speed of 10 mm min^{-1}, when the test in the program is started. This load was constantly increased until the pre-load of 30 N was reached.

Figure 32.: *Grips on the ZwickRoell RetroLine universal testing machine*

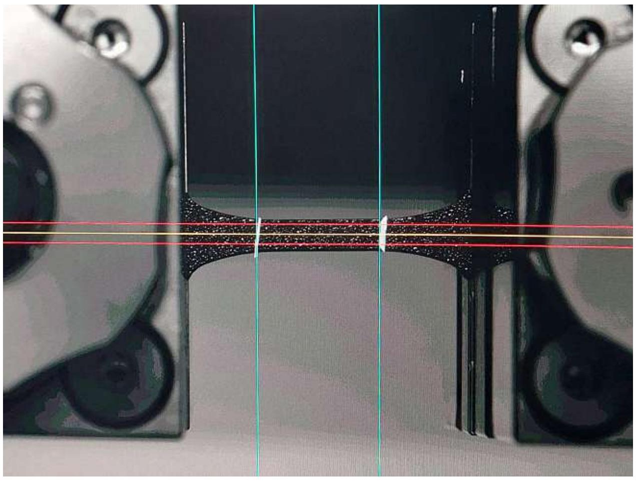

Figure 33.: *Automatic detection of the white marks on the sample by the video extensometer within the testing software testXpert III*

Subsequently, the tensile test continued with a crosshead speed of $1\,\mathrm{mm\,min^{-1}}$ until a force shutdown threshold of 20 % of the maximum detected force was recorded. The crossbeam was then automatically re-positioned in the opposite direction of the movement during the test. The re-positioning stopped, when the load on the sample was reduced to nearly 0 N. This ensured that by re-opening the grips no unwanted and unexpected movement of the sample would possibly harm the operator, the machine, or the sample.

The travel data were recorded with a save interval of 1 µm for the determination of the Young's modulus and until the breaking point with a save interval of 10 µm. The results of the material characteristics were then exported to a *Microsoft Excel Spreadsheet* (*xlsx*) file. This includes the raw data as well as the material characteristics and statistics, which were already calculated by the program.

3.5.3. Calculation

Material Properties

For the data analysis a *Medtool script* was used. It read the *PuTTY* logfile, containing the data of the five tested samples, and converted it to five separate *csv files*. A graph was then generated based on the raw data. The graph represents the force-displacement curve for each sample, an average curve, and the average maximum axial stiffness, k, as well as the average ultimate force, F_u.

This force-displacement diagram was converted into a stress-strain-diagram. This was done to express the material properties of the samples in a more generalized way. For this purpose the following formulas were applied to the force and the displacement data. The results were the stress, σ, and the strain, ε:

$$\sigma = \frac{F}{A_0} \tag{12}$$

and

$$\varepsilon = \frac{\Delta L}{L_0} \tag{13}$$

with the force, F, and the initial cross-sectional area of the sample in the gauge region, A_0. This area is calculated based on the measured dimensions of the 3D printed samples. The increment of elongation, ΔL, is derived from the displacement data and the initial gauge length, $L_0 = 15\,\mathrm{mm}$, can be taken from Figure 29. Instead of the initial gauge length, L_0, the clamping distance, $\hat{L}_0$, can be used to calculate the strain.

For the sake of simplicity, the elongation, ΔL, is be assumed to be equal to the displacement data, u, from the testing machine after application of the pre-load. The tensile strength, R_m, is calculated as the ultimate force, F_u, divided by the cross-sectional area. The Young's modulus, E, is calculated from the stress-strain diagram as the maximum slope, skipping the first 5 % of the data. This leads to the elimination of eventual fluctuations of the load in the beginning of the test.

T-Test

A t-test was employed to have a statistical evaluation of the test results. It was important to gain information whether the difference of the means obtained from both universal testing machines is of statistical significance. Therefore, an independent two-sample two-tailed test was performed, as both groups (i. e. the test series on the *MT-02* and the one on the *ZwickRoell*) did not depend on one another. The t-value and the p-value are needed to make assumptions about the statistical significance. The test statistic, the t-value, can be compared to a critical value given for a certain significance level. If its magnitude exceeds the critical value, the hypothesis for which is being tested is rejected. The p-value represents the significance of the test results. A value close to zero indicates high significance and with an increasing value, the level of significance drops [35]. The calculation of these values with the results of the tensile strength obtained by both universal testing machines were done with the statistical software *SPSS*.

4. Results

4.1. Final Material Testing System

A picture of the final MT-02 universal material testing machine is shown in Figure 34. The machine with the dimensions of 488 mm x 406 mm x 770 mm can be used for tensile and compression testing with loads up to 3.5 kN.

The current load during testing and the ultimate load after a test are shown on the touch screen. This serves as a quick preview of the results. If the whole measurement data (time, stepper movement, force) is of interest, this information can be exported via a USB port for further processing. Furthermore, this port is used to calibrate the load cell.

Figure 34.: *Built MT-02 testing machine*

4.2. Material Test Results

Five 3D printed samples were successfully tested on both systems (*MT-02* and *ZwickRoell*). The results of the tensile test series with the *MT-02* are depicted in Figure 35.

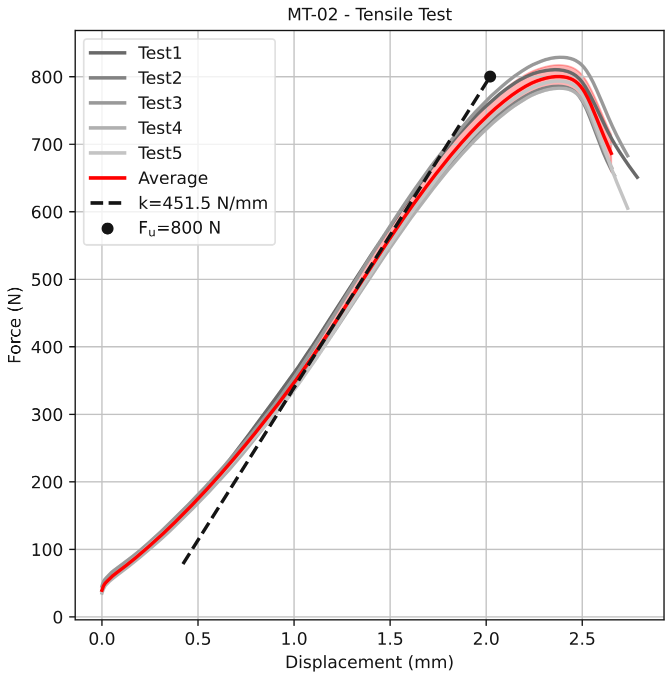

Figure 35.: *Force-displacement data of the five tests with 3D printed PETG samples on the MT-02 including the average curve (red), the ultimate force,* F_u*, and the stiffness,* k*, of the average curve; the standard deviation is sketched as a red area*

The stiffness, k, is visualized as a tangent to the average curve (red line) of the five tested samples at the point, where the maximum stiffness is measured. The red area indicates the standard deviation of the five measurements. The average ultimate load, F_u, marks the end point of the stiffness tangent. This is represented as a black dot and is the average of all ultimate loads. At the beginning of the curve (displacement $= 0$ mm), the force is not zero due to the application of the pre-load. The displacement data were only recorded after the load exceeded 30 N.

The graph in Figure 36 shows the computed stress (based on the initial cross-sectional area) and strain (based on $L_0 = 15$ mm). Additionally, it shows the Young's modulus, E , and the ultimate tensile strength, σ_u.

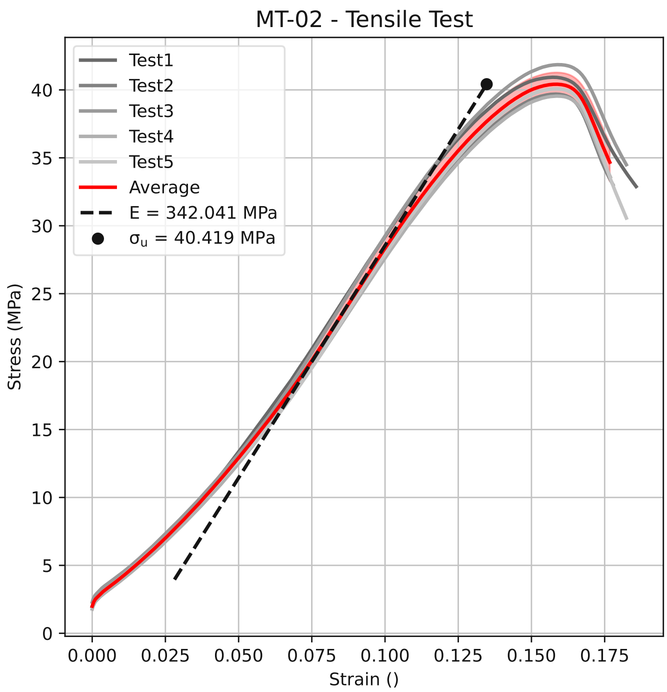

Figure 36.: *Stess-strain curve of the five tests with PETG on the MT-02 including the average curve (red), the tensile strength, σ_u, and the Young's modulus, E, of the average curve; the standard deviation is sketched as a red area*

Figure 37 shows the stress-strain curve of the test series with the *ZwickRoell*, using video extensometer measurements. This graph was created with *medtool 4.8* as well. Therefore, the value of the Young's modulus, E, is calculated with *medtool 4.8* and differs slightly from the value obtained by the testing software *testXpert III* from *ZwickRoell*. This discrepancy is based on slightly different methods of calculation.

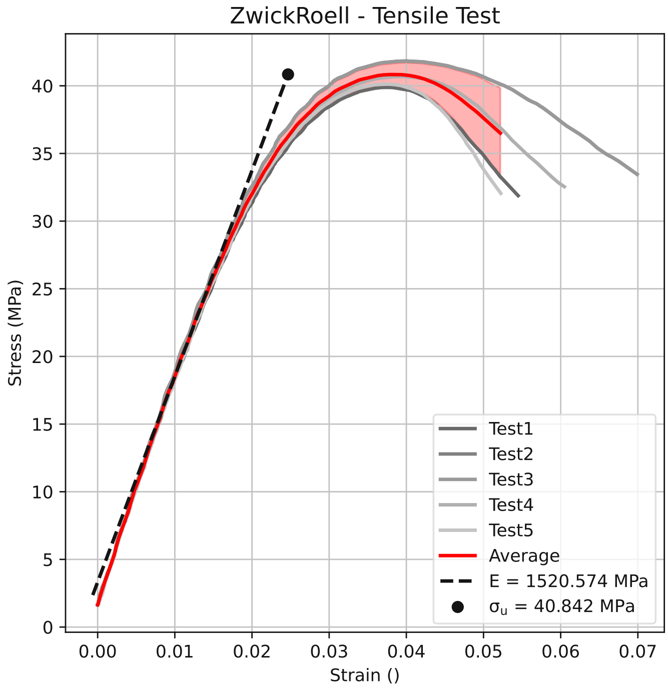

Figure 37.: *Stess-strain curve of the five tests on the ZwickRoell UTM with PETG using the video extensometer including the average curve (red), the tensile strength, σ_u, and the Young's modulus, E, of the average curve; the standard deviation is sketched as a red area*

The data obtained by the *ZwickRoell* UTM are analyzed based on the crosshead travel distance as well. This ensures that similar methods are used for the comparison of the testing results of the *MT-02* and the *ZwickRoell* UTM. The corrected tensile strength and the Young's modulus (based on the clamping distance instead of the gauge length) are computed to be $R_\mathrm{m} = 40.419\,\mathrm{MPa}$ and $E = 0.717\,\mathrm{GPa}$ for the *MT-02*. The respective values for the *ZwickRoell* UTM are calculated to be $R_\mathrm{m} = 40.642\,\mathrm{MPa}$ and $E = 1.901\,\mathrm{GPa}$.

More data about the strain of the samples are presented in Table 2. The change in length measured after the test is based on the minimum measured value in the gauge region. Informative quantities obtained from the test series with the *ZwickRoell* UTM are presented in Table 3 and Table 4.

Table 5 lists the results of both test series, with the *MT-02* (corrected values) and the *ZwickRoell* UTM. It shows that the corrected results, obtained by the *ZwickRoell* UTM, based on the crosshead travel distance with the clamping distance (CD), and the results with the video extensometer (EX) are similar. The strain values of the CD method are slightly underestimated, yielding an overestimated value of the Young's modulus by 28 % in comparison to the EX method.

It is observable that the stress values of the *MT-02* are similar to those of the *ZwickRoell* EX, but the uncorrected strain values are overestimated by a factor of over four. The corrected values with the clamping distance instead of the gauge length coincide with the values obtained by the *ZwickRoell* UTM much better. This results in the ultimate strain being off by a factor of two. The Young's modulus increased from 0.342 GPa to 0.717 GPa due to the correction. This results in a discrepancy from the *ZwickRoell* EX values of 48 %.

A picture of the fifth broken sample from each testing series is given in Figure 38. The white marks for the video extensometer are visible on the longer sample, which was used for the *ZwickRoell* UTM.

A two-sample t-test is used to compare the means of the tensile strengths extracted from both test series. The applied two-tailed test is examining for equality with a confidence of 95 %. The degrees of freedom are calculated to be 8 based on the five samples per test series. The p-value is computed to be 0.690. The t-value is calculated to be 0.413. This indicates that the difference between the means of both test series is not statistically significant.

Table 2.: *Results from the MT-02 based on the clamping distance including the values of the individual tests, the average, $\bar{x}$, and the standard deviation, σ, of the total uniform extension, A_{gt}, the total strain at break, A_t, as well as the change in length, ΔL, in width, Δa, and in depth, Δb, of the samples after the test*

MT-02	A_{gt} (%)	A_t (%)	ΔL (%)	Δa (%)	Δb (%)
Test 1	7.515	8.862	2.213	−11.364	−2.222
Test 2	7.554	8.484	2.213	−9.091	−2.222
Test 3	7.592	8.703	1.811	−9.091	−2.222
Test 4	7.678	8.441	2.012	−9.091	−2.222
Test 5	7.565	8.703	2.012	−11.364	−2.222
$\bar{x}$	7.581	8.639	2.052	−10	−2.222
σ	0.061	0.174	0.168	1.245	0.000

Table 3.: *Results from the ZwickRoell UTM with the video extensometer including the values of the individual tests, the average, $\bar{x}$, and the standard deviation, σ, of the Young's modulus, E, the tensile strength, R_m, the ultimate force, F_u, as well as the change in length, ΔL, in width, Δa, and in depth, Δb, of the samples after the test*

ZwickRoell	E (GPa)	R_m (MPa)	F_u (N)	ΔL (%)	Δa (%)	Δb (%)
Test 1	1.448	39.885	834.783	0.978	−7.692	−4.348
Test 2	1.475	40.713	852.113	0.978	−5.495	−6.522
Test 3	1.537	41.833	875.557	1.117	−7.692	−4.348
Test 4	1.480	40.684	851.508	0.838	−9.890	−6.522
Test 5	1.474	40.127	839.851	0.838	−7.692	−4.348
$\bar{x}$	1.483	40.648	850.762	0.950	−7.692	−5.217
σ	0.033	0.752	15.745	0.117	1.554	1.191

Table 4.: *Results from the ZwickRoell UTM including the values of the individual tests, the average, $\bar{x}$, and the standard deviation, σ, of the total uniform extension, A_{gt}, and the total strain at break without, A, as well as with the elastic part, A_{t}, using the video extensometer and the crosshead travel distance ($\hat{A}_{\mathrm{gt}}$, $\hat{A}_{\mathrm{t}}$)*

ZwickRoell	A_{gt} (%)	A (%)	A_{t} (%)	$\hat{A}_{\mathrm{gt}}$ (%)	$\hat{A}_{\mathrm{t}}$ (%)
Test 1	3.775	3.494	5.449	3.093	3.723
Test 2	3.945	4.380	6.360	3.159	3.941
Test 3	3.989	5.029	6.990	3.179	3.980
Test 4	3.927	4.077	6.047	3.199	3.895
Test 5	3.708	3.275	5.224	3.086	3.616
$\bar{x}$	3.869	4.051	6.014	3.143	3.831
σ	0.121	0.703	0.710	0.051	0.155

Table 5.: *Averages of five tensile tests per machine of the Young's modulus, E, the tensile strength, R_{m}, the ultimate strain, ε_u, the ultimate load, F_{u}, the initial cross-sectional area, A_0, and the clamping distance, $\hat{L}_0$, using the corrected values with the crosshead travel distance (CD) and the values with the video extensometer (EX)*

UTM	E (GPa)	R_{m} (MPa)	ε_{u} (%)	F_{u} (N)	A_0 (mm^2)	$\hat{L}_0$ (mm)
MT-02 CD	0.717	40.419	7.581	800.346	19.80	31.44
ZwickRoell CD	1.901	40.842	3.143	850.762	20.93	42.435
ZwickRoell EX	1.483	40.842	3.869	850.762	20.93	

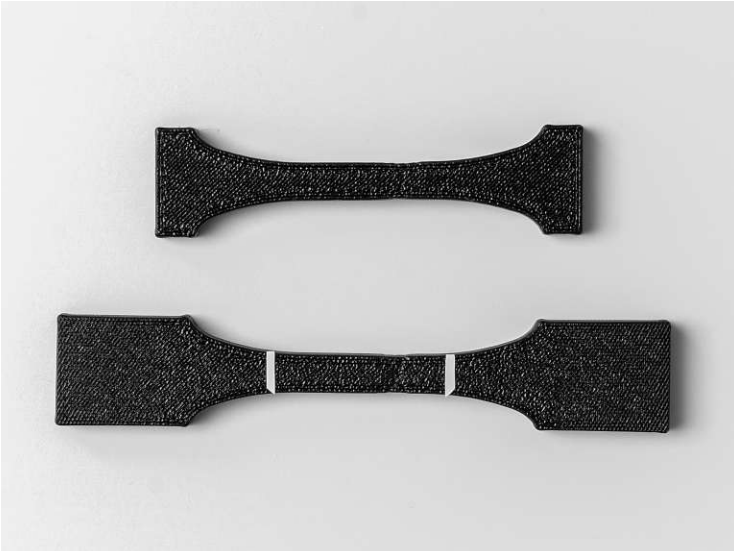

Figure 38.: *Samples after the tensile test: sample for the MT-02 on the top and the one for the ZwickRoell with the markers for the video extensometer on the bottom*

5. Discussion and Conclusion

This thesis presents a design of a material testing machine with the intention of being used for practical applications in teaching or for demonstration purposes. The requirements for the machine were easy extensibility, portability, intuitive operation, and a moderate price. The built machine, *MT-02*, fulfills all those demands, while providing an acceptable precision and accuracy regarding the load data.

The *MT-02* allows tensile tests or compression tests without laborious preparations and displays the results in a simple way. Thus, this machine represents a practical tool for understanding material testing as well as the interpretation of the results regarding the material properties. It should be unproblematic to replicate this machine in facilities, where it is needed. This can be emphasized, as the machine was built at a technical university by using the available machines, tools, and only open-source software.

5.1. Design Features

The focus was always on simplicity and intuitive operation during the process of designing the universal testing machine. The use of the TFT LCD touch screen allows a clear display of all modes, preferences, and results. Furthermore, practically everyone in our society nowadays is familiar to using touch screens, whether on smartphones, automated teller machines, or ticket machines. Therefore, the operation of the *MT-02* should come naturally to the user. The USB-B port as well as the on/off switch are located in the front of the machine. This prevents the user from an unnecessarily long search for the power button or for where to insert what type of USB cable. On the other hand, the location of the power plug protects the plug from being broken off easily. This was achieved by placing the power plug rather towards the back of the machine, close to the column, and beneath the stepper driver case.

The steppers are situated on top of the machine, far from any other potential heat source. This facilitates the reduction of generated heat. Ventilation slots are incorporated in the housings of the stepper drivers and the *Arduino* as well as the one for the shield, the PCB, and the modules. These prevent overheating of the electrical devices. Overall, the housings are designed in a rather open way but still ensuring that fragile parts are protected from unintentional impacts.

5.2. Material Test Result Comparison

In general, it can be stated that the results concerning the stresses obtained by the *MT-02* are very similar to those recorded by the *ZwickRoell* UTM. However, the values of the strain and the Young's modulus do not lie within an acceptable range compared to the values obtained by the video extensometer and by the crosshead travel distance of the *ZwickRoell* UTM.

The method with the video extensometer is considered as the more precise method, as it is not influenced by the compliance of the machine itself. The *ZwickRoell* data were analyzed based on the crosshead travel distance as well, despite having the accurate strain data from the video extensometer. This ensures that the data from the *MT-02* are not only compared to precise values, but also to values obtained by a similar method. Furthermore, the results obtained by the crosshead travel distance were corrected based on the clamping distance instead of the initial gauge length. This correction yields results with a discrepancy of 19 % concerning the strain and 28 % for the Young's modulus in comparison to the *ZwickRoell* EX data. It is important to note that the calculation of the Young's modulus differs slightly due to the use of different software.

Concerning the *MT-02*, the corrected results reveal closer compliance to the values of the *ZwickRoell* data regarding the strain and thus the Young's modulus. Nevertheless, the value of the ultimate stain and Young's modulus are still off compared to the *ZwickRoell* video extensometer results by 96 % and 48 %, respectively. In comparison, the uncorrected value of the Young's modulus of the *MT-02* is underestimated by 77 %. The tensile strength of the *MT-02* test represents a slightly lower value (1 % discrepancy) compared to the value of the *ZwickRoell* results.

Higher ultimate forces were recorded on the *ZwickRoell* UTM in contrast to the *MT-02*. However, similar stresses were computed for all samples. This discrepancy can be explained by the different cross-sectional areas of both sample types. Although both sample types are designed with the same geometry in the gauge region, the 3D printed samples show different cross-sectional areas due to a lacking calibration of the 3D printer. The cross-sectional area in the gauge region of the sample for the *MT-02* with 19.8 mm^2 was 5.4 % smaller than the one for the *ZwickRoell* UTM with 20.93 mm^2. Nevertheless, similar tensile strengths are computed, as the actual measured dimensions were used for the calculation of the data.

The strains calculated with the corrected *MT-02* crosshead travel data are roughly twice as large as the ones obtained by the *ZwickRoell* UTM. This discrepancy in elongation can be ascribed to the compliance of the machine and the clamps themselves. Conducting a test with a rigid test sample and recording the distance the crosshead travels without actually causing any strain in the rigid sample provides a correction factor. It is also possible to use a camera with digital image correlation to track the exact displacement of the sample in its region of interest, without the influence of the compliance of the machine.

5.3. Possible Improvements

In retrospect, a simplified design and construction process could have been achieved by integrating the bearings directly into the mounts. Furthermore, the gearbox on the stepper motor made the mounting of the stepper motor much more complicated. The mounting surface area was reduced due to the gearbox. The stepper motor mount could be simplified by choosing a more powerful stepper motor without a gearbox.

The handling of the machine could be facilitated by using a bigger touch screen with increased button and font sizes. This would decrease the likelihood of involuntarily touching the wrong button and could increase the overall user experience. This would be especially beneficial, when working with groups of students or spectators, allowing everyone to read the testing results more easily.

5.4. Ideas of Extension

An automatic testing mode could be of interest in addition to the already implemented tensile testing and compression testing. Moreover, an automated application of a pre-load with a subsequent manual test would offer a more consistent way of testing. Such a semi-automated mode could also implement an automated return of the crosshead to the initial position or to a position, where the load again drops to zero. Ideally the testing modes could even be extended with cyclic testing. To implement all these methods only a modification of the *Arduino* code is needed, no additions to the existing hardware are required.

A ruler with an adjustable marker could be integrated into the column. This would help to obtain a more intuitive idea of the displacement of the crosshead during the test. The marker could be used to mark the initial position of the crosshead, allowing to analogously read the travel distance. This setup could be achieved in a cheap and simple way, using additive manufacturing and attaching it through the groove of the column.

Bibliography

[1] ZwickRoell GmbH und Co. KG. *AllroundLine Z250 SN/SW/SH/SE materials testing machines*. accessed on: 29.05.2024. 2023. URL: www.zwickroell.com/fileadmin/content/Files/SharePoint/user_upload/PI_EN/02_757_AllroundLine_Z250_Materials_Testing_Machine_PI_EN.pdf.

[2] Illinois Tool Works Inc. *6800 Series - Universal Testing Systems*. accessed on: 29.05.2024. 2024. URL: www.instron.com/en/products/testing-systems/universal-testing-systems/low-force-universal-testing-systems/-/media/literature-library/products/2020/01/6800-series-universal-testing-systems.pdf?.

[3] S. Hermann. *Open-Pull*. accessed on: 18.05.2024. June 2020. URL: https://github.com/CNCKitchen/Open-Pull.

[4] X. Zhang. *Universal Tensile Testing Machine VERSION TWO*. accessed on: 18.05.2024. 2020. URL: www.instructables.com/Universal-Tensile-Testing-Machine-VERSION-TWO/.

[5] L. Schöggl. *Praxishandbuch Werkstoffprüfung: Methoden der zerstörenden und zerstörungsfreien Werkstoffprüfung*. 2. Ausgabe. Brunn am Gebirge: TÜV Austria Fachverlag, 2018. ISBN: 978-3-901942-99-0.

[6] H.-J. Bargel. "Werkstoffprüfung". In: *Werkstoffkunde: Strukturen - grundlegende Eigenschaften*. Ed. by H.-J. Bargel. 13th ed. Springer-Lehrbuch. Berlin, Germany: Springer-Verlag GmbH, 2022. ISBN: 978-3-662-63961-0. DOI: 10.1007/978-3-662-63961-0.

[7] *DIN 50125: Testing of metallic materials - Tensile test pieces*. Tech. rep. Deutsches Institut für Normung, Aug. 2022. DOI: 10.31030/3337825.

[8] *DIN 50106: Testing of metallic materials - Compression test at room temperature*. Tech. rep. Deutsches Institut für Normung, Feb. 2023. DOI: 10.31030/3393741.

[9] *ISO 527-1: Plastics — Determination of tensile properties — Part 1: General principles*. Tech. rep. International Organization for Standardization, July 2019.

[10] L. Krüger, P. Trubitz, and S. Henschel. "Bruchmechanisches Verhalten unter quasistatischer und dynamischer Beanspruchung". In: *Moderne Methoden der Werkstoffprüfung*. Ed. by H. Biermann and L. Krüger. Wiley Online Library, 2014, pp. 1–52. DOI: 10.1002/9783527670673.ch1.

[11] B. Wittbrodt and J. M. Pearce. "The effects of PLA color on material properties of 3-D printed components". In: *Additive Manufacturing* 8 (2015), pp. 110–116. ISSN: 2214-8604. DOI: 10.1016/j.addma.2015.09.006.

[12] *Standard Test Method for Tensile Properties of Plastics*. Standard. West Conshohocken, PA, USA: ASTM International, Mar. 2015.

[13] I. Faridmehr, M. H. Osman, A. B. Adnan, A. F. Nejad, R. Hodjati, and M. Azimi. "Correlation between engineering stress-strain and true stress-strain curve". In: *American Journal of Civil Engineering and Architecture* 2.1 (2014), pp. 53–59. DOI: 10.12691/ajcea-2-1-6.

[14] M. Rahman, D. Patterson, A. Cheok, and R. Betz. "Motor Drives". In: *Power Electronics Handbook*. Ed. by M. H. Rashid. Third Edition. Boston: Butterworth-Heinemann, 2011, pp. 915–991. ISBN: 978-0-12-382036-5. DOI: 10.1016/B978-0-12-382036-5.00034-3.

[15] V. M. Hernández-Guzmán, R. Silva-Ortigoza, and J. A. Orrante-Sakanassi. *Bipolar Permanent Magnet Stepper Motor*. Advances in Industrial Control. Cham, Switzerland: Springer Nature Switzerland AG, 2021, pp. 361–391. ISBN: 978-3-030-58786-4. DOI: 10.1007/978-3-030-58786-4.

[16] C. Brecher and M. Weck. *Machine Tools Production Systems 3 : Mechatronic Systems, Control and Automation*. 1st ed. 2022. Lecture Notes in Production Engineering. Wiesbaden: Springer Fachmedien Wiesbaden Imprint: Springer, 2022. ISBN: 3658346221. URL: 10.1007/978-3-658-34622-5.

[17] *Stepper Motor 17HS19-1684S-PG19*. STEPPERONLINE Inc. New York, USA, May 2023. URL: www.omc-stepperonline.com/index.php?route=product/product/get_file&file=185/17HS19-1684S-PG19_Full_Datasheet.pdf.

[18] K. Berns, A. Köpper, and B. Schürmann. *Technische Grundlagen Eingebetteter Systeme*. Wiesbaden, Germany: Springer Vieweg, 2019. ISBN: 978-3-658-26516-8. DOI: 10.1007/978-3-658-26516-8.

[19] H. Czichos. "Maschinenbau". In: *Mechatronik*. Wiesbaden: Springer Fachmedien Wiesbaden, 2015, pp. 189–206. ISBN: 978-3-658-09949-7. DOI: 10.1007/978-3-658-09950-3.

[20] *DM542T(V4.0)*. 4.0. STEPPERONLINE Inc. New York, USA, Oct. 2020. URL: www.omc-stepperonline.com/index.php?route=product/product/get_file&file=382/DM542T_V4.0.pdf.

[21] *A4988 Stepper Motor Driver Carrier, Black Edition*. Pololu Corporation. 2024. URL: www.pololu.com/file/0J450/a4988_DMOS_microstepping_driver_with_translator.pdf.

[22] J. Ctibor and I. Pazdera. "The new stepper driver for low-cost Arduino based 3D printer with dynamic stepper control". In: *Mechatronics 2017: Recent Technological and Scientific Advances*. Ed. by T. Březina and R. Jabłoński. Springer International Publishing AG, 2018, pp. 458–466. ISBN: 978-3-319-65960-2. DOI: 10.1007/978-3-319-65960-2.

[23] *A4988: DMOS Microstepping Driver with Translator And Overcurrent Protection*. Rev. 8. 4988-DS. Allegro MicroSystems, LLC. Apr. 2022. URL: www.allegromicro.com/-/media/files/datasheets/a4988-datasheet.pdf.

[24] D. Mitra. *How to Improve Motion Smoothness and Accuracy of Stepper Motors*. Texas Instruments Incorporated. Dallas, Texas, Oct. 2021. URL: www.ti.com/lit/an/sloa293a/sloa293a.pdf.

[25] U. Sommer. *Arduino: Mikrocontroller-Programmierung mit Arduino/Freeduino*. Haar bei München: Franzis, 2013. ISBN: 978-3-645-65147-9.

[26] C. Kühnel. *Arduino : das umfassende Handbuch*. 1. Auflage. Bonn: Rheinwerk Verlag, 2020. ISBN: 978-3-8362-7345-9.

[27] Arduino. *UNO R3*. accessed on: 04.06.2024. 2022. URL: docs.arduino.cc/hardware/uno-rev3/.

[28] Arduino. *Arduino Hardware*. accessed on: 04.06.2024. 2022. URL: www.arduino.cc/en/hardware.

[29] M. E. Miller. "LCD Display Technology". In: *Color in Electronic Display Systems: Advantages of Multi-primary Displays*. Cham: Springer Nature Switzerland AG, 2019, pp. 87–105. ISBN: 978-3-030-02834-3. DOI: 10.1007/978-3-030-02834-3_5. URL: https://doi.org/10.1007/978-3-030-02834-3_5.

[30] K. Mitzner. "Chapter 1 - Introduction to PCB Design and CAD". In: *Complete PCB Design Using OrCAD Capture and PCB Editor*. Ed. by K. Mitzner. Boston: Newnes, 2009, pp. 1–13. ISBN: 978-0-7506-8971-7. DOI: 10.1016/B978-0-7506-8971-7.00001-9. URL: www.sciencedirect.com/science/article/pii/B9780750689717000019.

[31] ALM Intelligent Technology (Suzhou) Co.,Limited. *12mm 16mm SFU1204 SFU1604 SFU1605 Ball Screw*. accessed on: 03.04.2024. Suzhou, China, 2018. URL: www.autolinearmotion.com/12mm-16mm-sfu1204-sfu1604-sfu1605-ball-screw.html.

[32] H. Karlsen. *Library: UTFT*. accessed on: 25.04.2024. 2018. URL: www.rinkydinkelectronics.com/library.php?id=51.

[33] H. Karlsen. *Library: URTouch*. accessed on: 25.04.2024. 2018. URL: www.rinkydinkelectronics.com/library.php?id=92.

[34] D. Pahr. *Downloads*. accessed on: 24.04.2024. Pfaffstätten, Austria, 2024. URL: www.dr-pahr.at/medtool/?page_id=25.

[35] B. Rosner. *Fundamentals of Biostatistics*. 7th ed. Brooks/Cole, 2011. ISBN: 978-0-538-73349-6.

[36] *INA219 Zerø-Drift, Bidirectional Current/Power Monitor With I2C Interface*. SBOS448G. Revised December 2015. Texas Instruments Incorporated. Aug. 2008. URL: www.ti.com/lit/gpn/ina219.

A. Appendix

A.1. Bill of Materials

The following tables list the parts (Table 6), screws (Table 7), tools, and machines (Table 8) needed to build the *MT-02*.

Table 6.: *Parts needed for the assembly*

Count	**Part**
2	Aluminum profile 40 mm x 80 mm x 590 mm
3	Aluminum profile 40 mm x 80 mm x 400 mm
1	Aluminum profile 40 mm x 80 mm x 320 mm
1	Aluminum profile 40 mm x 80 mm x 300 mm
4	Corner bracket
34	Slot nuts M8
1	Aluminum flat bar 10 mm x 70 mm x 500 mm
1	Aluminum flat bar 6 mm x 70 mm x 500 mm
1	Load cell (500 kg)
2	Stepper motor + gearbox 19:1
2	Coupler 8 mm to 10 mm
2	Ball screw set 500 mm (SFU 1605)
1	Arduino Mega
1	TFT-LCD touch screen 3.2 in
1	Shield for TFT-LCD touch screen
2	Stepper Driver DM542T
1	24 V to 5 V converter
1	Load cell amplifier HX711
1	Power supply 24 V, 8 A
1	PETG filament
1	TPU filament
	Crimp connectors
	Headers

Table 7.: *Screws needed for the assembly*

Count	Dimensions	Type
4	M3x6 mm	slotted screw
8	M3x10 mm	countersunk screw
2	M3x20 mm	slotted screw
2	M3x35 mm	slotted screw
2	M4x10 mm	slotted screw
12	M5x20 mm	hex screw
8	M5x30 mm	hex screw
8	M5x35 mm	hex screw
8	M8x16 mm	raised countersunk screw
26	M8x20 mm	countersunk screw
8	M8x45 mm	hex screw
8	M8x70 mm	hex screw
1	M12x35 mm	countersunk screw

Table 8.: *Tools and machines needed for the assembly*

Tools
2 mm hex key
2.5 mm hex key long
4 mm hex key
5 mm hex key
6 mm hex key
13 mm nut socket wrench
Circlip Pliers
Lubricant
Files
Crimp set
Soldering set

Machines
3D printer
milling machine
drilling machine

A.2. Discarded Design-Ideas

Some ideas came up during the process of designing the machine, that were tried out but ended up as dead ends. Below, the intentions behind the ideas and their eventual issues are stated.

A.2.1. Different Stepper Drivers

The A4988 module and the DM320T digital stepper driver were used before choosing the DM542T as the ideal stepper driver for this specific application.

A4988 Module

The idea behind the A4988 module was to make use of its advantages. It is very small and cheap but should provide a sufficient amount of power for the stepper motor [17, 23]. Nevertheless, the maximum speed was too low and the chip would get quite hot, even after only half a minute of moving the crosshead.

DM320T Digital Stepper Driver

Using the DM320T driver increased the adequacy while not increasing the size of the stepper driver too much. However, the rotational speed of the stepper motors was not precise. At some specific speed ranges the speed of the crosshead increased by a factor of approximately 100. Therefore, the needed accuracy of the testing speed while performing a measurement could not be fulfilled and a different digital stepper driver, the DM542T, was chosen and used in the final design.

A.2.2. Stepper Position Alignment

An overall misalignment of both ball screws can lead to a skew of the crosshead accompanied by unequal load distributions and damage to the machine. This might happen due to the stepper motor skipping a step. Therefore, a specific function was programmed. This function aligned both ball screws using the top beam for reference. The current through the coils of the motors was limited to 0.5 A to prevent any damage to the machine only for the alignment function. Eventually, this function was removed, as the current can only be changed mechanically on the DM542T stepper driver.

A.2.3. Current Measurement

The INA219 chip measures current. It uses an inter-integrated circuit (I2C) interface to communicate with the *Arduino*. This communication is done via two pins: SCL and SDA. Each INA219 module must have its own unique address on the I^2C bus. So, the specific contacts on the second module have to be bridged with the help of a soldering iron. This is specified in the datasheet of the chip [36].

Two modules are then connected in parallel to the *Arduino* SCL and SDA with a pull up resistor of 3.3 kΩ for each pin [36]. In order to use both modules simultaneously with different addresses, the following in line 166 in the Adafruit library Adafruit_INA219.h has to be changed from:

`Adafruit_INA219(uint8_t addr = INA219_ADDRESS);`

to

`Adafruit_INA219(uint8_t addr = INA219_CALC_ADDRESS);`

One module was connected to one motor, respectively, to measure its current flowing through one coil. The idea was to detect a missing step, by looking for an abnormal jump in the current curve. However, the module appeared not to be precise enough for this application, as no missing steps could be detected.

A.2.4. Relay Module

Replacing the Mechanical Switches of the Digital Driver

A relay module was used to replace the dual inline package (DIP) switches in the *DM320T* digital stepper driver. This facilitated the change of the current and the microstep resolution of the stepper motors with the help of the *Arduino* microcontroller.

The lowest current setting on the *DM320T* digital stepper driver is defined by the first three switches being turned on. So, the default setting for all switches was set to be on. Therefore, the normally closed terminal was used along with the common terminal. This means that if the input signal, which controls the relay, was set high (or was not connected), both pins of the switch were connected. Hence, the high input signal represented the same state as if the DIP switch was on. The input signal simply had to be set to low to get the state of the switch being off.

This idea worked like intended, but was very inconvenient to execute. The stepper driver had to be unscrewed, the DIP switch desoldered, and wires soldered on connecting the relay module to the stepper driver (Figure 39). Furthermore, the *DM320T* stepper driver did not behave as expected regarding the speed of the stepper motors. As a consequence, this idea was not replicated with the *DM542T* stepper driver.

Disabling the Digital Drivers while the Arduino is Starting

Unwanted current is flowing through the coils of the stepper motors, while the *Arduino* microcontroller is starting. A relay was used to disable the stepper driver until the *Arduino* was fully done with its setup.

The normally opened terminal was used to realize this configuration. This ensured that the stepper driver was not connected to the voltage supply, when the microcontroller could not provide a proper input signal yet.

This configuration worked well but was not used for the final design of the machine. This setup was only intended to be an additional feature and to make use of a free

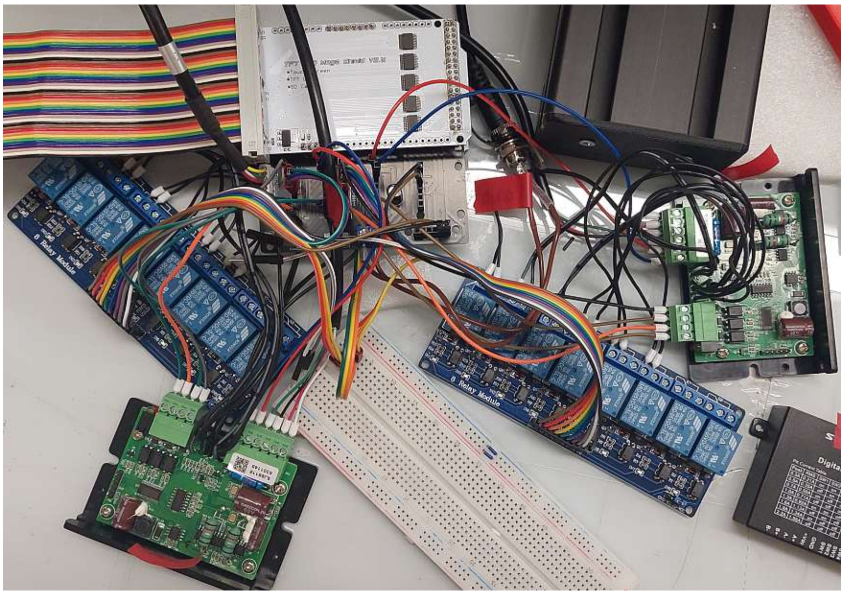

Figure 39.: *8-channel relay modules along with the unscrewed DM320T digital stepper drivers*

relay in the 8-channel relay module. When the idea with the replacement of the DIP switches was dropped, it was also decided not to use this setup.